Application of Finite Difference Time Domain Technique to Left-Handed Materials

Işıl Nurdan Işık

Submitted to the
Institute of Graduate Studies and Research
in Partial Fulfillment of the Requirements for the Degree of

Master of Science
in
Electrical and Electronic Engineering

Eastern Mediterranean University
November 2013
Gazimağusa, North Cyprus

Approval of the Institute of Graduate Studies and Research

Prof. Dr. Elvan Yılmaz
Director

I certify that this thesis satisfies the requirements as a thesis for the degree of Master of Science in Electrical and Electronic Engineering.

Prof. Dr. Aykut Hocanın
Chair, Department of Electrical and Electronic Engineering

We certify that we have read this thesis and that in our opinion it is fully adequate in scope and quality as a thesis for the degree of Master of Science in Electrical and Electronic Engineering.

Assist. Prof. Dr. Rasime Uyguroğlu
Supervisor

Examining Committee

1. Prof. Dr. Şener Uysal

2. Assoc. Prof. Dr. Hasan Demirel

3. Asst. Prof. Dr. Rasime Uyguroğlu

ABSTRACT

The aim of this thesis is to simulate left handed materials (metamaterials) by using the finite difference time domain (FDTD) method. One dimensional (1D) simulations are carried out using Matlab and for two dimensional (2D), MTM-FDTD Virtual Tool is used.

FDTD method is used for 1D and 2D simulations to observe wave behavior in metamaterial slab.

1D simulation of air-dielectric-air media were studied for comparison with 1D air-metamaterial-air simulation. In 1D air-dielectric-air simulation, reflection, transmission and a decreased in wave amplitude were observed as wave propagated through the dielectric slab with positive refractive index whereas in 1D air-metamaterial-air simulation exponentially growing wave has been occurred in the metamaterial slab which have a negative refractive index. Also, no reflection was observed in this simulation, therefore, making the simulation successful in meeting the theory.

2D simulations were studied in air-metamaterial-air media by defining different negative refractive indexes for the metamaterial slabs. Different scenarios were tested, the perfect lens behavior was observed with metamaterial slabs having refractive index -1 and all results were found to be consistent with other studies in the literature.

Keywords: Metamaterials, Finite Difference Time Domain (FDTD), Perfect Lens, Negative Refractive Index, Left-Handed Materials

ÖZ

Bu tezin amacı zamanda sonlu farklar (FDTD) yöntemini kullanarak metamalzemelerin simüle edilmesidir. Bir boyutlu (1B) simülasyonlar Matlab kullanılarak, iki boyutlu (2B) simülasyonlar MTM-FDTD sanal aracı kullanılarak yapılmıştır.

Zamanda sonlu farklar yöntemi, metamalzeme içerikli levhanın içindeki dalga hareketini gözlemlemek için kullanılmıştır.

1B hava-metamalzeme-hava simülasyonu ile karşılaştırma yapabilmek amacıyla 1B hava-dielektrik-hava simülasyonu çalışılmıştır. 1B hava-dielektrik-hava simülasyonunda elektromanyetik dalga pozitif kırılma indisi olan dielektrik ortamdan geçerken yansıma, iletim ve dalga yüksekliğinde düşüş gözlenmiştir. Oysa 1B hava-metamalzame-hava simülasyonunda negatif kırılma indisi olan metamalzeme içerisinde katlanarak büyüyen dalga oluşmuş ve bu simülasyonda hiç yansıma gözlemlenmemiştir. Bu sonuçlar simülasyonların teori ile uyumlu ve başarılı olduğunu göstermiştir.

Metamalzemeler için değişik negatif kırılma indisleri tanımlanarak 2B hava-metamalzeme-hava simülasyonları çalışılmıştır. Değişik senaryolar tasarlanıp, simüle edilmiş, negatif kırılma indisi -1 olan metamalzemelerle mükemmel lens davranışı gözlemlenmiş ve sonuçlar literatürdeki çalışmalarla tutarlı bulunmuştur.

Anahtar Kelimeler: Metamalzemeler, Zamanda Sonlu Farklar Yöntemi (FDTD), Mükemmel Lens, Negatif Kırılma İndisi, Sol-Elli Materyaller

To my daddy

ACKNOWLEDGMENTS

I would like to thank my supervisor Assist. Prof. Dr. Rasime Uyguroğlu for her support and guidance throughout my thesis research. I learned from her a lot.

I wish to thank all of the faculty members in the department of Electrical and Electronic Engineering especially the chairman of the department Prof. Dr. Aykut Hocanın.

I would like to express my deepest appreciation to Prof. Dr. Haluk U. Tosun who treated me as my father from the beginning of my undergraduate education to present. I would not be able to complete myself without him.

My special thanks to Assist. Prof. Dr. Emine Atasoylu who was with me unlimitedly when I was down and felt unable to finish. She believed in me, lifted me up, guided me, encouraged me and showed me why I actually was here.

I would like to thank Prof. Dr. Şener Uysal and Assoc. Prof. Dr. Hasan Demirel for their help to complete my study.

Deepest thanks to all of my family members. Thanks to my mommy, aunt and their families. Special thanks to my uncle and his family for their endless support. Also, thanks to the ones who became my sisters. My huge family never gave up on me. I felt their love and support in everyday of my life.

I want to thank my friends for all the time we went through together and the ones who helped me a lot to complete my study, one by one thanks to all of the research assistants and all of the special people in my life for shaping me to stand where I’m standing now.

Finally, I would like to thank my daddy. I wish he could have been here with me.

TABLE OF CONTENTS

LIST OF TABLES

LIST OF FIGURES

LIST OF SYMBOLS AND ABBREVIATIONS

E: Electric Field

H: Magnetic Field

ε: Permittivity

μ: Permeability

ε_r: Relative Permittivity

μ_r: Relative Permeability

1D: 1 Dimensional

2D: 2 Dimensional

ABC: Absorbing Boundary Condition

BW: Backward Wave

CFL: Courant-Friedrichs-Levy Stability Criterion

DNG: Double-Negative

DPS: Double-Positive

ENG: Epsilon-Negative

FDTD: Finite Difference Time Domain

LHM: Left-handed Material

MNG: Mu-Negative

Ssd: Source-Slab Distance

St: Slab Thickness

Chapter 1

INTRODUCTION

1.1 General Introduction

Scientists work on understanding materials which certainly goes beyond understanding what is on their surface. The difficult process of understanding the internal structure and properties of materials becomes essential when engineers are trying to use them especially to invent or design new technology.

Since internal structure and properties of materials become important to design new technology that is why engineers and scientists work on designing materials which have properties that cannot be found in natural materials.

During the past decade, there has been an increasing interest in ‘metamaterials’. These are artificial materials with the ability to engineer electromagnetic and optical properties which cannot be found in natural materials. The unconventional response functions of these metamaterials contain fabricated structures or composite materials with the known material responses but when brought together have a new physically realizable response that do not occur or may not be readily available in the nature.

Metamaterials are structured and have electromagnetic particles such as split-ring resonators and nanowires as their structural units as Pendry suggested in 1996 [1] and 1999 [2] to provide negative index materials according to their relative

permittivity and relative permeability. After the appropriate design of the electric and magnetic properties of these particles, it is possible to create materials with electromagnetic properties that are unknown for conventional materials.

Metamaterials with simultaneously negative permittivity and negative permeability are called left-handed materials. In early 1967, it was shown by the theoretical work of Veselago [3] how electromagnetic wave propagation will be in medium with simultaneously negative permittivity and negative permeability.

The first metamaterial particles are split-ring resonators and nanowires introduced by Pendry and enormous research in this field took place after a material with negative refractive index was fabricated for the first time in 2000 by David Smith and his research group [4] and experimental verification followed by the same research group.

The development of metamaterials has led to understand the optics with negative permittivity and negative permeability, including perfect lenses. This thesis will focus on metamaterials and how metamaterials behave as perfect lens.

Interest to metamaterials will continue since they enable the design of materials with new properties.

1.2 Thesis Objectives

The work presented in this thesis is focused on simulating left handed materials (metamaterials) by using the finite difference time domain (FDTD) method that is the numerical method of choice. One dimensional (1D) simulations are carried out using Matlab and for two dimensional (2D), MTM-FDTD Virtual Tool is used.

FDTD method will be used for 1D and 2D simulations to observe wave behavior in metamaterial slab.

In 1D simulations, air-metamaterial-air media and air-dielectric-air media will be investigated related to the wave propagation. The difference between wave behaviors in each media will be observed.

In 2D simulation of metamaterials, the difference between using point source and uniform plane wave will be observed by putting them in different places in the computational domain and wave behavior in metamaterial slab will be seen.

Different negative refractive indexes will be demonstrated and perfect focusing will be reached at the end of the simulations.

1.3 Thesis Contributions

The subject of this present thesis is to study wave propagation in the different media as air-dielectric-air and air-metamaterial-air media by using FDTD method. After realizing how wave behaves in different media by comparing dielectric and metamaterials slabs, the results obtained at the end of the study can be used for further research also experimentally and can form a background for realizing 3D simulations. The thesis also demonstrates the focusing with different refractive indexes and this will cause a better understanding in optics. Research on understanding metamaterials and their potential use will continue to be a hot topic for a long time.

1.4 Overview

The thesis consists of 5 chapters and is organized as follows, FDTD method will be introduced in Chapter 2, metamaterials will be reviewed in Chapter 3, the simulation will be demonstrated in Chapter 4, and results and conclusions will follow.

Chapter 2

FINITE DIFFERENCE TIME DOMAIN TECHNIQUE

For modeling computational electrodynamics finite difference time domain technique (FDTD) is used as a numerical tool. The solutions include a wide frequency range in order to be able to reach accuracy in a single run.

The FDTD method is versatile, powerful and has been widely used for modeling of electromagnetic wave interactions with various frequency materials. FDTD implementation is easy and conceptually simple. In this present study, to simulate electromagnetic wave-metamaterial interaction the FDTD equations are needed.

FDTD is a numerical modeling technique that uses a grid-based time domain to solve Maxwell's equations in a computational domain. FDTD is a direct solution of Maxwell's equations. Partial differential forms of Maxwell's equations are discretized using central-difference approximations with respect to time and space partial derivatives.

Since electromagnetic field is examined, FDTD equations are solved by the repeatable process. The electric field vector $\vec{E}$ with all 3 components can be solved instantly in time and the magnetic field vector $\vec{H}$ with all 3 components can be solved instantly in next time and the computation is repeated. Thus, FDTD is a time-

stepping method and it causes that the electromagnetic properties are updated at each time until it reaches steady-state.

This method was developed by Yee in 1966 [5]. In literature, it is well known that for discretization Yee's lattice is used. FDTD method stores different field components for different grid locations.

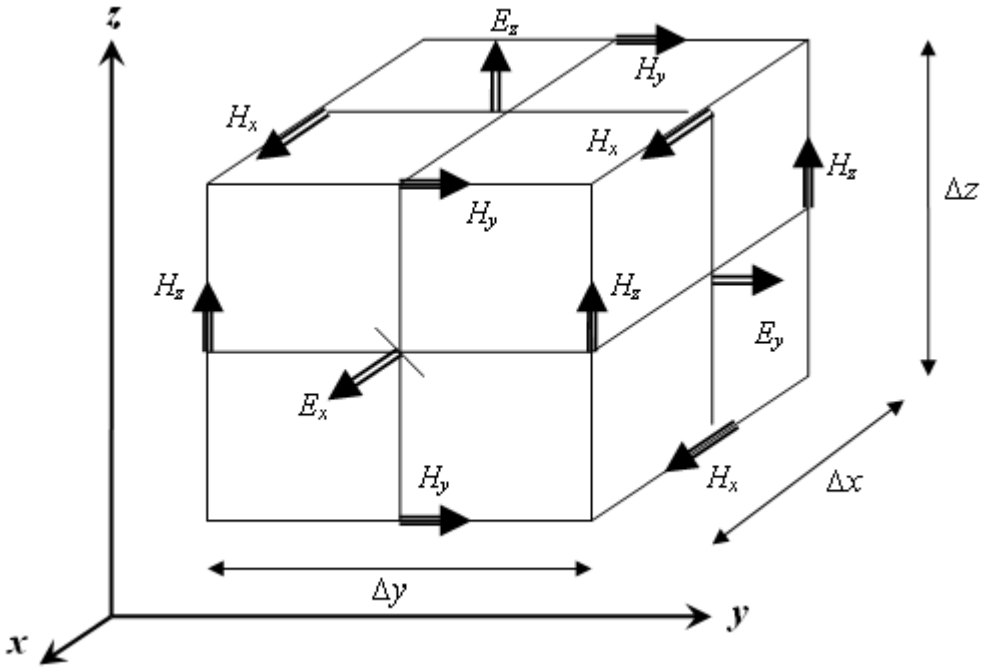

Figure 2.1. Yee's Lattice [5]

Positions of various field components are seen in Figure 2.1. The magnetic field components are in the middle of the edges and the electric field components are in the center of the faces.

Yee's algorithm:

All of the derivatives are replaced by finite differences according to time and space discretization. Resulting difference equations are solved to yield update equations that expresses present fields in terms of past fields. Then, magnetic and electric fields are evaluated. Magnetic and electric fields are repeatedly updated throughout the desired duration until steady-state is reached.

2.1 Maxwell's Equations

Maxwell's equations govern the propagation of field at any desirable structure so that the formulation of FDTD method starts with the differential form of Maxwell's equations. The medium is assumed to be linear, isotropic and homogeneous for the simplicity [6].

Equations 2.1 to 2.4 show the general Maxwell's equations [6];

$$\nabla x\vec{E} = -\frac{\partial \vec{B}}{\partial t} \tag{2.1}$$

$$\nabla x\vec{H} = \vec{J} + \frac{\partial \vec{D}}{\partial t} \tag{2.2}$$

$$\nabla .\vec{D} = \rho \tag{2.3}$$

$$\nabla .\vec{B} = 0 \tag{2.4}$$

where $\vec{E}$ is the electric field intensity vector, $\vec{B}$ is the magnetic flux density vector, $\vec{H}$ is the magnetic field intensity vector, $\vec{J}$ is the electric current density, $\vec{D}$ is the

electric flux density vector and ρ is the electric charge density. The 3D source free ($\bar{J} = 0$) Maxwell's equations of a homogeneous medium are given in equations 2.5 and 2.6:

For the electric field [7]:

$$\nabla x\vec{E} = -\mu\frac{d\vec{H}}{dt} \rightarrow \begin{cases} \frac{\partial E_z}{\partial y} - \frac{\partial E_y}{\partial z} = -\mu\frac{\partial H_x}{\partial t} \\ \frac{\partial E_x}{\partial z} - \frac{\partial E_z}{\partial x} = -\mu\frac{\partial H_y}{\partial t} \\ \frac{\partial E_y}{\partial x} - \frac{\partial E_x}{\partial y} = -\mu\frac{\partial H_z}{\partial t} \end{cases} \quad (2.5)$$

For the magnetic field [7]:

$$\nabla x\vec{H} = \varepsilon\frac{d\vec{E}}{dt} \rightarrow \begin{cases} \frac{\partial H_z}{\partial y} - \frac{\partial H_y}{\partial z} = \varepsilon\frac{\partial E_x}{\partial t} \\ \frac{\partial H_x}{\partial z} - \frac{\partial H_z}{\partial x} = \varepsilon\frac{\partial E_y}{\partial t} \\ \frac{\partial H_y}{\partial x} - \frac{\partial H_x}{\partial y} = \varepsilon\frac{\partial E_z}{\partial t} \end{cases} \quad (2.6)$$

FDTD method is a second order accurate, explicit method. To apply the FDTD method, firstly, Maxwell's equations are needed to be discretized according to the time and space derivatives.

For a function *u* of space and time:

$$u(x, y, z, t) = u(i\Delta x, j\Delta y, k\Delta z, n\Delta t) = u^n(i, j, k) \tag{2.7}$$

where Δt is the time increment, Δx, Δy, Δz are space increments in *x*, *y* and *z* directions; *n* denotes the current calculation time and *i, j, k* denote the space locations in the discretized domain.

Any time derivative can be approximated as:

$$\left.\frac{\partial u(x, y, z, t)}{\partial t}\right|_{t=n\Delta t} \approx \frac{u^{n+1/2}(i, j, k) - u^{n-1/2}(i, j, k)}{\Delta t} \tag{2.8}$$

And a space derivative can be approximated as:

$$\left.\frac{\partial u(x, y, z, t)}{\partial x}\right|_{x=i\Delta x} \approx \frac{u^n(i+1/2, j, k) - u^n(i-1/2, j, k)}{\Delta x} \tag{2.9}$$

u refers to E_x, E_y, E_z and H_x, H_y, H_z.

In this thesis, discretized forms of Maxwell's equations used for simulations are shown [7]:

For the electric field:

$$E_{x(i,j,k)}^{n+1} = E_{x(i,j,k)}^{n} + \frac{\Delta t}{\varepsilon \Delta y}\left(H_{z(i,j+1,k)}^{n+1/2} - H_{z(i,j,k)}^{n+1/2}\right) - \frac{\Delta t}{\varepsilon \Delta z}\left(H_{y(i,j,k+1)}^{n+1/2} - H_{y(i,j,k)}^{n+1/2}\right) \quad (2.10)$$

$$E_{y(i,j,k)}^{n+1} = E_{y(i,j,k)}^{n} + \frac{\Delta t}{\varepsilon \Delta z}\left(H_{x(i,j,k+1)}^{n+1/2} - H_{x(i,j,k)}^{n+1/2}\right) - \frac{\Delta t}{\varepsilon \Delta x}\left(H_{z(i+1,j,k)}^{n+1/2} - H_{z(i,j,k)}^{n+1/2}\right) \quad (2.11)$$

$$E_{z(i,j,k)}^{n+1} = E_{z(i,j,k)}^{n} + \frac{\Delta t}{\varepsilon \Delta x}\left(H_{y(i+1,j,k)}^{n+1/2} - H_{y(i,j,k)}^{n+1/2}\right) - \frac{\Delta t}{\varepsilon \Delta y}\left(H_{x(i,j+1,k)}^{n+1/2} - H_{x(i,j,k)}^{n+1/2}\right) \quad (2.12)$$

For the magnetic field:

$$H_{x(i,j,k)}^{n+1/2} = H_{x(i,j,k)}^{n-1/2} + \frac{\Delta t}{\mu \Delta z}\left(E_{y(i,j,k)}^{n} - E_{y(i,j,k-1)}^{n}\right) - \frac{\Delta t}{\mu \Delta y}\left(E_{z(i,j,k)}^{n} - E_{z(i,j-1,k)}^{n}\right) \quad (2.13)$$

$$H_{y(i,j,k)}^{n+1/2} = H_{y(i,j,k)}^{n-1/2} + \frac{\Delta t}{\mu \Delta x}\left(E_{z(i,j,k)}^{n} - E_{z(i-1,j,k)}^{n}\right) - \frac{\Delta t}{\mu \Delta z}\left(E_{x(i,j,k)}^{n} - E_{x(i,j,k-1)}^{n}\right) \quad (2.14)$$

$$H_{z(i,j,k)}^{n+1/2} = H_{z(i,j,k)}^{n-1/2} + \frac{\Delta t}{\mu \Delta y}\left(E_{x(i,j,k)}^{n} - E_{x(i,j-1,k)}^{n}\right) - \frac{\Delta t}{\mu \Delta x}\left(E_{y(i,j,k)}^{n} - E_{y(i-1,j,k)}^{n}\right) \quad (2.15)$$

Discretized forms of Maxwell's equations are given above with 3 components of either electric field intensity $\vec{E}$ as E_x, E_y and E_z or magnetic field intensity $\vec{H}$ as H_x, H_y and H_z for 3D case.

In 1D simulations, equations 2.10 and 2.14, in 2D simulations equations 2.12, 2.14 and 2.15 are modified according to the cases.

For 1D, the electric field component is defined as:

$$E_x^{n+1}(k) = E_x^n(k) - \frac{\Delta t}{\varepsilon \Delta z}[H_y^{n+1/2}(k+1) - H_y^{n+1/2}(k)] \qquad (2.16)$$

The magnetic field component is defined as:

$$H_y^{n+1/2}(k) = E_y^{n-1/2}(k) - \frac{\Delta t}{\mu \Delta z}[E_x^n(k) - E_x^n(k-1)] \qquad (2.17)$$

2.2 Absorbing Boundary Conditions

The computer's memory and storage capacity are limited, therefore a computational domain must be defined with limited size when using the FDTD method for simulation. Also appropriate boundary conditions must be defined. Absorbing boundary conditions (ABC) allow electromagnetic waves to propagate out of the computational domain, so that they don't interfere with the fields inside. One of the most important concerns of the FDTD method is the requirement of boundary conditions as they theoretically absorb fields. Imperfect ABC's create reflections and the accuracy of the FDTD method depends on the accuracy of the ABC's [8].

In this thesis, ABC's are defined according to Mur's absorbing boundary conditions to update computational domain.

Mur's absorbing boundary conditions at the first electric field node on the left and last electric field on the right, respectively:

$$E_x\big|_M^{n+1} = E_x\big|_M^{n-1} + \frac{c\Delta t - \Delta z}{c\Delta t + \Delta z}\left(E_x\big|_{M-1}^{n+1} - E_x\big|_M^{n}\right) \tag{2.18}$$

$$E_x\big|_1^{n+1} = E_x\big|_2^{n-1} + \frac{c\Delta t - \Delta z}{c\Delta t + \Delta z}\left(E_x\big|_2^{n+1} - E_x\big|_1^{n}\right) \tag{2.19}$$

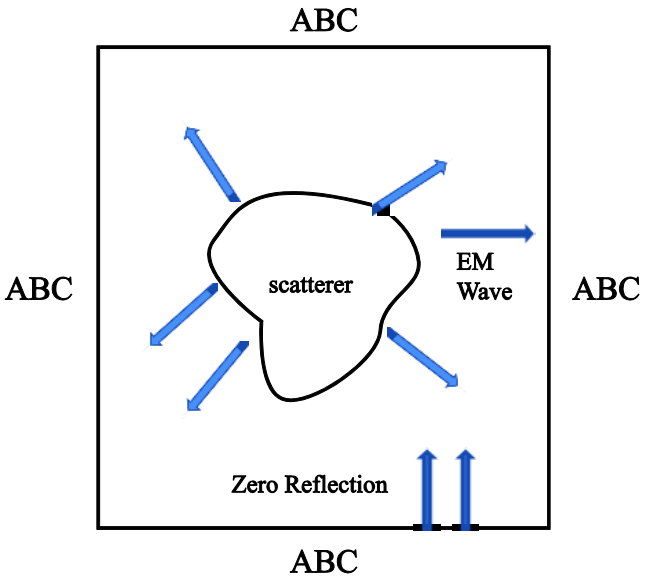

Figure 2.2. Absorbing Boundary Conditions

Figure 2.2 demonstrates a computational domain sided with absorbing boundary conditions, in the middle, there is an object and electromagnetic waves are propagating inside the computational domain. Also there is no reflection at the boundaries.

2.3 Space Cell Sizes

Determination of the cell sizes and the time step size are two important aspects of the FDTD method. Cell sizes must be small enough to achieve accurate results at the highest frequency of interest. The cell sizes must be much less than the smallest possible wavelength to reach accurate results.

$$\Delta_{max} \leq \frac{\lambda}{10} \tag{2.20}$$

λ is the minimum possible wavelength which corresponds to the highest frequency.

The structure of the medium made of and the field variation are important to determine step sizes. The time step, required for FDTD algorithm, has to be bounded relative to the space sizes. This bound is necessary to prevent numerical instability.

2.4 Stability

Maxwell's equations 2.5 and 2.6 require a special bound that the time increment Δt and the space increments Δx, Δy, Δz which are relative to each other. These increments are related as it is given in equation 2.21.

$$\Delta t \leq \frac{1}{c\sqrt{(\frac{1}{\Delta x^2}+\frac{1}{\Delta y^2}+\frac{1}{\Delta z^2})}} \tag{2.21}$$

This equation is known as Courant-Freidrichs-Lewy (CFL) Stability Criterion [7]. According to the CFL Stability Criterion, when

$$\Delta tc > \frac{1}{\sqrt{(\frac{1}{\Delta x^2}+\frac{1}{\Delta y^2}+\frac{1}{\Delta z^2})}} \tag{2.22}$$

numerical instability occurs. Therefore, step sizes are chosen based on the equation 2.21.

The two universal constants of nature;

$\varepsilon_0 = \frac{1}{36\pi} x10^{-9}$ F/m and $\mu_0 = 4\pi x10^{-7}$ H/m are called the electric permittivity of free space and the magnetic permeability of free space, respectively, where the permittivity and the permeability are:

$$\varepsilon = \varepsilon_0 \varepsilon_r \text{ and } \mu = \mu_0 \mu_r \tag{2.23}$$

where ε_r and μ_r are the relative permittivity and relative permeability, respectively and c is the speed of electromagnetic wave related to the permittivity and the permeability [7].

$$c = \frac{1}{\sqrt{\varepsilon_0 \mu_0}} \cong 3x10^8 \quad \text{m/s} \tag{2.24}$$

Chapter 3

METAMATERIALS

3.1 Definitions

Metamaterials are in general defined as artificial materials showing properties that are not available in nature. They gain their properties from their structure. Typically, they have periodical structures obtained by many identical resonant scattering objects.

Pendry & Smith [9] defined metamaterials by pointing out common essential properties as: “Materials made out of carefully fashioned microscopic structures can have electromagnetic properties unlike any naturally occurring substance. In particular, these metamaterials can have a negative index of refraction”.

The Virtual Institute for Artificial Electromagnetic Materials and Metamaterials [10] gives a flexible definition by also pointing out that it is both incomplete and too strict: “Metamaterial is an arrangement of artificial structural elements, designed to achieve advantageous and unusual electromagnetic properties”.

When different definitions of metamaterials are analyzed, it is obvious that there is not a single definition but one can talk about metamaterials having distinguishable properties that are not observed in the constituent materials and not observed in nature [11].

Materials with negative relative permittivity and relative permeability (metamaterials) are also named as:

- Left-handed media (also known as Veselago media)
- Backward-wave media (BW Media)
- Double-negative (DNG) metamaterials
- Media with negative refractive index

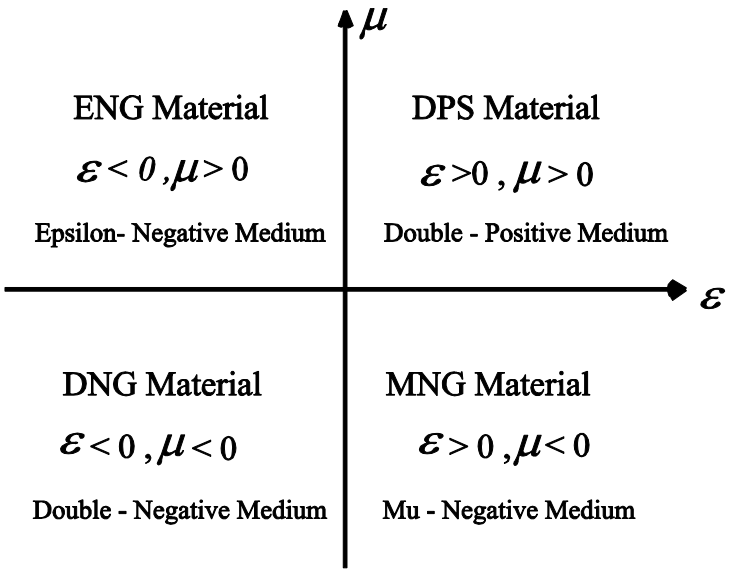

Figure 3.1. Materials Classification [12]

Media are classified according to their microscopic parameters. A medium with permittivity and permeability both greater than zero ($\varepsilon>0$, $\mu>0$) is called double-positive medium (DPS), a medium with permittivity less than zero and permeability greater than zero ($\varepsilon<0$, $\mu>0$) is called epsilon-negative medium (ENG), a medium with permeability less than zero and permittivity greater than zero ($\varepsilon>0$, $\mu<0$) is called mu-negative (MNG) medium, and a medium with both permittivity and

permeability less than zero (ε<0, μ<0) is called double-negative (DNG) medium [11]. The illustration of these media can be seen in Figure 3.1.

3.2 Reflection and Refraction in DPS Medium

This thesis will focus on metamaterials and how metamaterials behave as perfect lens. To explain this, firstly reflection and refraction will be demonstrated in the general case.

Reflection and refraction of plane waves are shown in Figure 3.2. Here two linear, isotropic and homogeneous media are separated by a plane surface S.

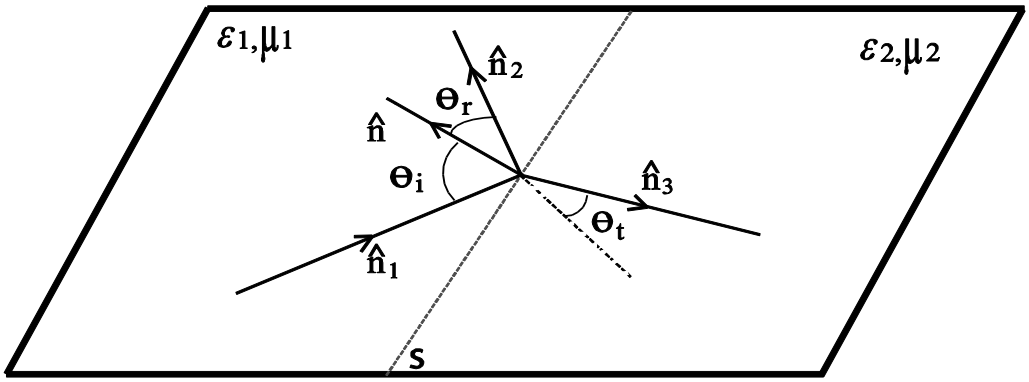

Figure 3.2. Reflection and Refraction at a Dielectric Interface [13]

The first medium has parameters ε_1 and μ_1. When a plane wave propagates in this medium in the direction of $\hat{n}_1$ it becomes an incident on the interface S. The reflected wave moves in the direction of $\hat{n}_2$ and the refracted wave continuous to the second media with ε_2 and μ_2 in the direction of $\hat{n}_3$.

The angles between unit normal vector $\hat{n}$ and interface S are:

- *The angle of incidence* which is defined as the angle θ_i between $\hat{n}$ and $-\hat{n}_1 (0 \leq \theta_i \leq \pi/2)$,
- *The angle of reflection* is the angle θ_r between $\hat{n}$ and $\hat{n}_2$,
- *The angle of refraction* is the angle θ_t between -$\hat{n}$ and $\hat{n}_3$.

Snell's law [14] proves that $\hat{n}$, $\hat{n}_1$, $\hat{n}_2$ and $\hat{n}_3$ are *coplanar*, meaning that $\hat{n}_2$ and $\hat{n}_3$ also lie in the plane of incident, which the plane is formed by $\hat{n}$ and $\hat{n}_1$ vectors.

Snell's phase matching procedure also leads to $\sin\theta_i = \sin\theta_r$ and $\theta_i = \theta_r$. This is the Snell's law of reflection; the angle of incidence is equal to the angle of reflection.

Snell's law of refraction leads to the index of refraction, *n*;

$$k_1 \sin\theta_i = k_2 \sin\theta_t \tag{3.1}$$

$$\frac{\sin\theta_t}{\sin\theta_i} = \frac{k_1}{k_2} \tag{3.2}$$

where k is the wave number.

Since the velocities of propagation in the two media are:

$$v_1 = \frac{1}{\sqrt{\varepsilon_1 \mu_1}} \tag{3.3}$$

$$v_2 = \frac{1}{\sqrt{\varepsilon_2 \mu_2}} \tag{3.4}$$

and the wave numbers are:

$$k_1 = w\sqrt{\varepsilon_1 \mu_1} \tag{3.5}$$

$$k_2 = w\sqrt{\varepsilon_2 \mu_2} \tag{3.6}$$

in medium 1 and medium 2, respectively.

$$\sqrt{\frac{\varepsilon_1\mu_1}{\varepsilon_2\mu_2}} = \frac{v_2}{v_1} = n \tag{3.7}$$

Then

$$\frac{\sin\theta_t}{\sin\theta_i} = \frac{v_2}{v_1} = n \tag{3.8}$$

The angle of refraction is determined by the refractive index which is a product of ε and μ, and Snell's law where the same parameter ratios determine the impedance and the amount of waves reflected-transmitted.

3.3 Reflection and Refraction in DNG Medium

Metamaterials are designed to achieve negative relative permittivity and negative relative permeability. In 1967, Veselago showed that if relative permittivity and relative permeability are both negative then refractive index *n*, must also take negative sign. Materials with both negative relative permittivity and negative relative permeability are called negative-index materials. Figure 3.3 shows the transmissions through positive and negative index materials.

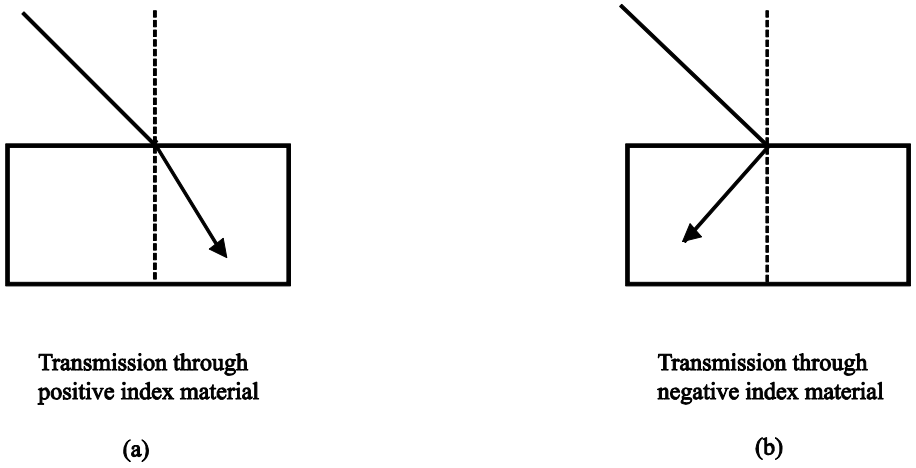

Figure 3.3. Transmissions through Positive (a) and Negative (b) Index Materials [9]

$n = \sqrt{\varepsilon\mu}$ and has to take its negative sign but the Snell's Law is still valid.

$$n_1 \sin\theta_i = n_2 \sin\theta_t \tag{3.9}$$

Since n_2 is negative, the rays will be reflected on the same side of the normal, when entering the metamaterials.

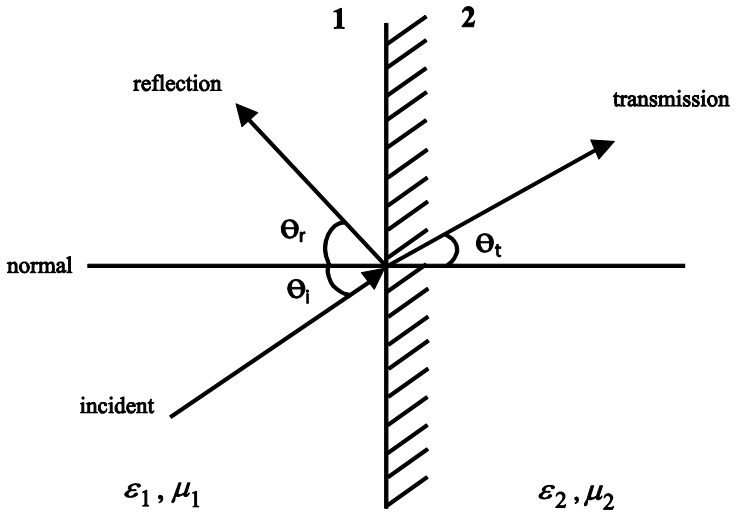

Figure 3.4. Reflection and Refraction in DNG Medium

Figure 3.4 shows the reflection and refraction in double-negative medium. Incident wave propagating in first medium and reflected in first medium again with having a negative angle with the surface normal and transmitted to the second medium.

3.4 Perfect Lens

Conventional lenses will focus the light beam coming from a focal point and travelling through the lens to another focal point following the lens. Object at a distance L_1 from the lens is converging by the lens to a real image at a distance L_2

after the lens. A point source at a focal point propagates waves from the object and is converted by the lens to a real image.

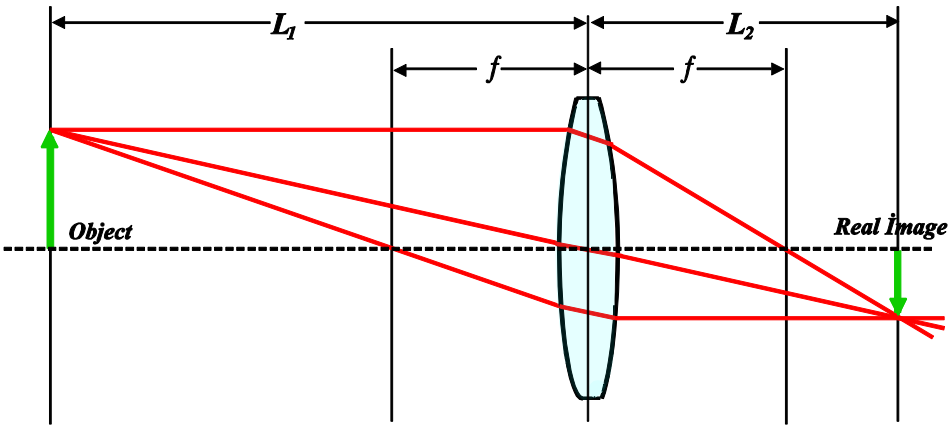

Figure 3.5. Conventional Lens [15]

Figure 3.5 demonstrates that an object is placed at a distance L_1 and the image is real at a distance L_2, inversed and smaller than the object where $L_1 > L_2$. When $L_1 = L_2$ then image will be real, inversed and same size with the object.

The resolution of an image obtained with conventional lenses is limited by the wavelength of light. These lenses cannot focus light onto an area smaller than a square wavelength. Pendry proposed lens called a superlens (or perfect lens) that overcomes the traditional limitation of conventional lens performance. Pendry's unconventional lenses are lenses with negative refractive index.

A superlens is shown in Figure 3.6, where the slab is a slab with negative refractive index equal to -1 (n=-1). It has a thickness d and placed at a distance d/2 from the light source. The light inside the medium makes a negative angle with the surface normal and converges back to a point within the slab. The light reaches focus again

at a distance d/2 after leaving the slab. This is true for the case that both ε and μ are -*1* and that the refractive index $n = -\sqrt{\varepsilon\mu}$ has the negative square root. The impedance of the medium $Z = \sqrt{\frac{\mu}{\varepsilon}}$ keeps its positive sign. When ε=-1 and μ=-1 the medium is a perfect match to air (or free space) and the interfaces show no reflection.

This is the case of both interfaces (air-metamaterial and metamaterial-air surfaces) causing the light to be perfectly transmitted into free space (air).

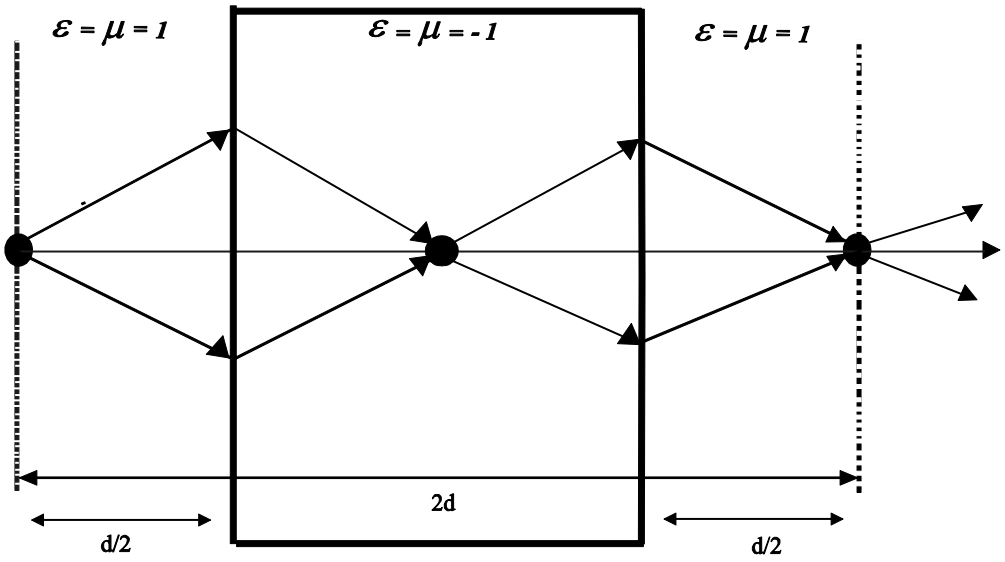

Figure 3.6. Perfect Lens [16]

Pendry [16] made use of Veselago's theoretical study on negative refractive materials and concluded that a medium with negative refractive index can act as a perfect lens. What he meant by the perfect lens was that an image can be refracted to the other side of the medium exactly the same as it is and even with a higher resolution wherein conventional lenses or positive index lenses this is not possible.

The perfect lens is demonstrated in Figure 3.6. Here the light from an object placed on the left side of the negative index lens (slab, metamaterial) is refracted at the surface, the image is reversed inside the lens and the light is refracted again to form an image the same as the object on the right side of the lens. This is only possible when the refractive index (n), relative permittivity (ε_r) and relative permeability (μ_r) are all negative. For a higher resolution it is suggested [9] that all must take the value -1.

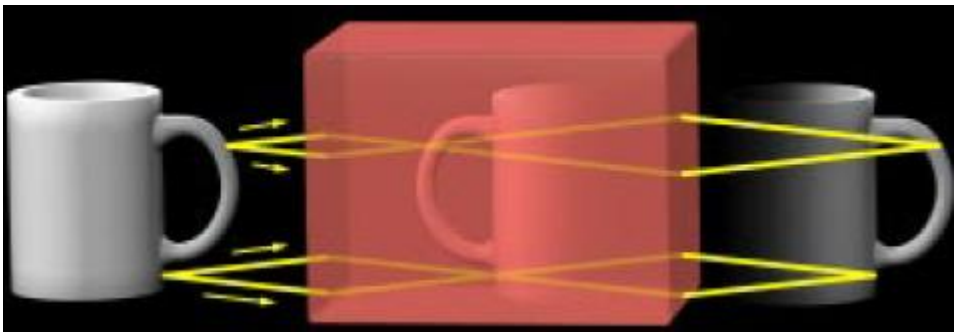

Figure 3.7. Demonstration of the Perfect Lens [9]

Figure 3.7 shows that when the object was placed to the left side of the slab, the image is real after the slab with same distances to slab.

Analytically, transmission and reflection coefficients are calculated according to materials (air-metamaterial-air). The calculation of transmission and reflection coefficients is as shown below.

In the conventional materials, in normal incidence case, reflection and transmission coefficients with angle of incidence and angle of refraction equal to zero are given in equations 3.10 and 3.11 respectively.

$\theta_i = 0$ and $\theta_t = 0$ then;

$$\Gamma = \frac{\eta_2 - \eta_1}{\eta_2 + \eta_1} \tag{3.10}$$

$$T = \frac{2\eta_2}{\eta_2 + \eta_1} \tag{3.11}$$

Whereas in LHM the reflection and transmission coefficients are as follows:

$$\Gamma = \frac{\eta_2 - \eta_1}{\eta_2 + \eta_1} \frac{1 - e^{-jk_2 d}}{1 - [(\eta_2 - \eta_1)/(\eta_2 + \eta_1)]^2 e^{-jk_2 d}} \tag{3.12}$$

$$T = \frac{4\eta_2 \eta_1}{(\eta_2 + \eta_1)^2} \frac{e^{-jk_2 d}}{1 - [(\eta_2 - \eta_1)/(\eta_2 + \eta_1)]^2 e^{-jk_2 d}} \tag{3.13}$$

Impedance matching gives that there is no reflection Γ=0 and full transmission $T = e^{-j2k_2 d}$ will occur in the perfect lens [12].

Chapter 4

SIMULATIONS OF METAMATERIALS

4.1 Definition of Problem

In this present thesis, simulation of metamaterials will be observed. The problem is defined in semi-infinite medium as slab and wave behavior which will be investigated in different slabs such as dielectric and metamaterial slabs.

Problem configuration is set to see how the wave behavior is in different media. In computational domain, 3 media are assumed as shown in Figure 4.1.

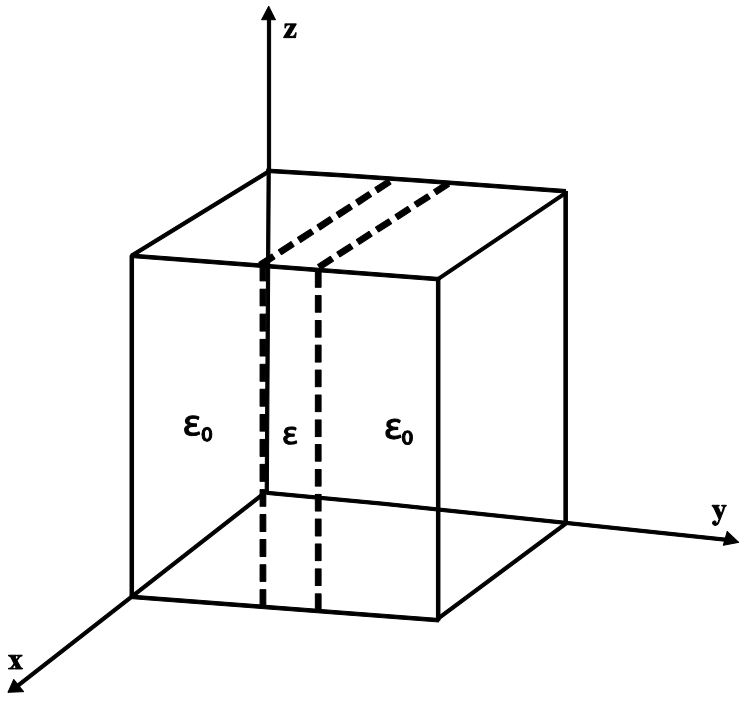

Figure 4.1. 3D Configuration of the Air-Slab-Air Structure

Media are defined as air, metamaterial, air, respectively in 1D and 2D simulations. For 1D simulation of wave behavior in dielectric slab instead of metamaterial slab, dielectric slab is placed in the middle of the computational domain. For 1D simulation slabs are placed to the middle of the computational domain between the steps 80-120. Slab thickness is defined as 1.5 cm which corresponds to $\lambda/20$ and slab to source distances is defined as 0.75 cm which corresponds to $\lambda/40$ for 2D simulations.

4.2 1D Simulation of Dielectric Slab

The 1D FDTD wave propagation program has been modified to be used through air-dielectric-air media. Air-dielectric-air media were studied for comparison with the wave behavior in air-metamaterial-air media.

In 1D FDTD air-dielectric-air wave interaction program, computational domain was divided into 3 media. First medium is air, then, a dielectric slab has been placed into the middle of the computational domain and third medium is air.

Some coefficients such as permittivities, permeabilities, the step size and time increment was defined according to the media of concern in the program.

The permittivity of free space is defined as ε_0, permeability of free space is defined as μ_0, the step size is chosen to be Δx=37.7 mm. The time step size is obtained by using the stability criterion as $\Delta t=\Delta x/2c$. Both media 1 and 3 consist of free space and the parameters used is the same. In medium 2, dielectric slab parameters are defined as $\varepsilon_r = 4$, $\mu_r = 1$.

Discretized forms of Maxwell's equations (eqn's 2.16&2.17) are used for 1D simulation of wave interaction in air-dielectric-air medium.

Wave behavior can be seen in different time steps as shown in Figure 4.2.

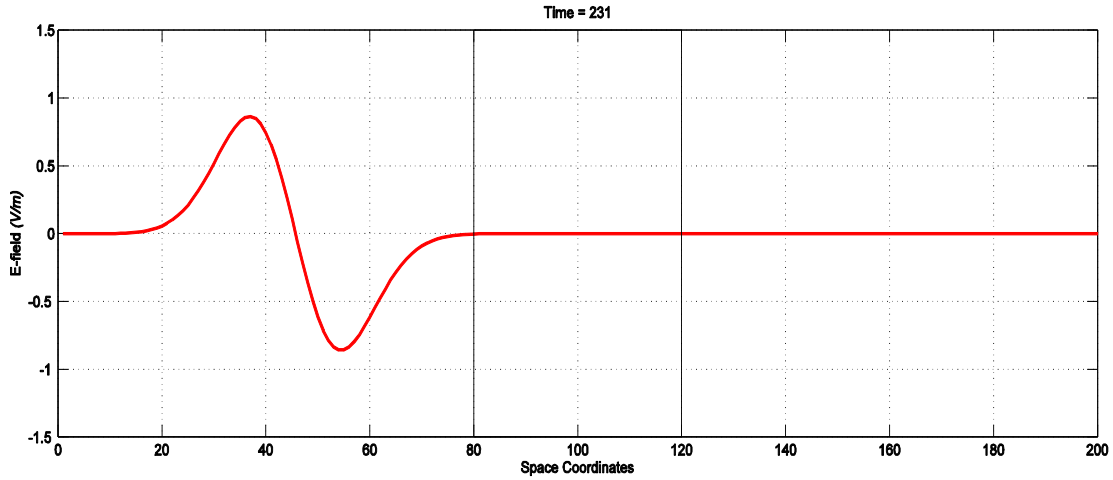

(a) wave starts to propagate in air medium

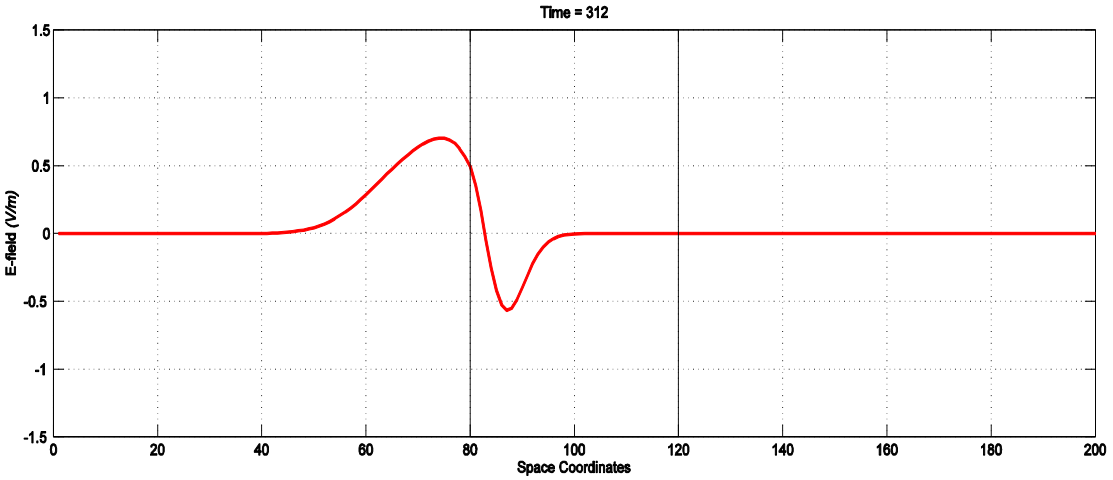

b) wave hits the dielectric slab

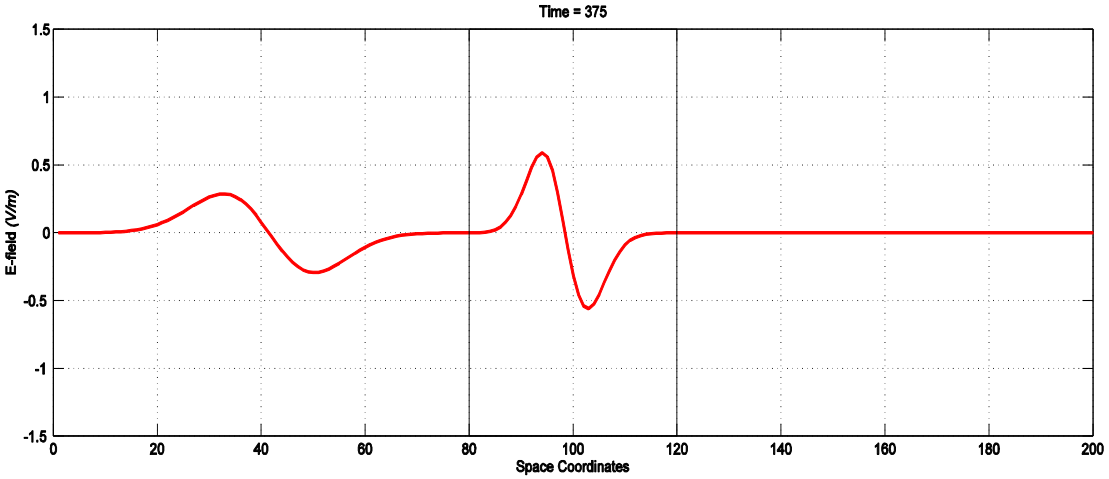

(c) inside the slab wave decreases in amplitude

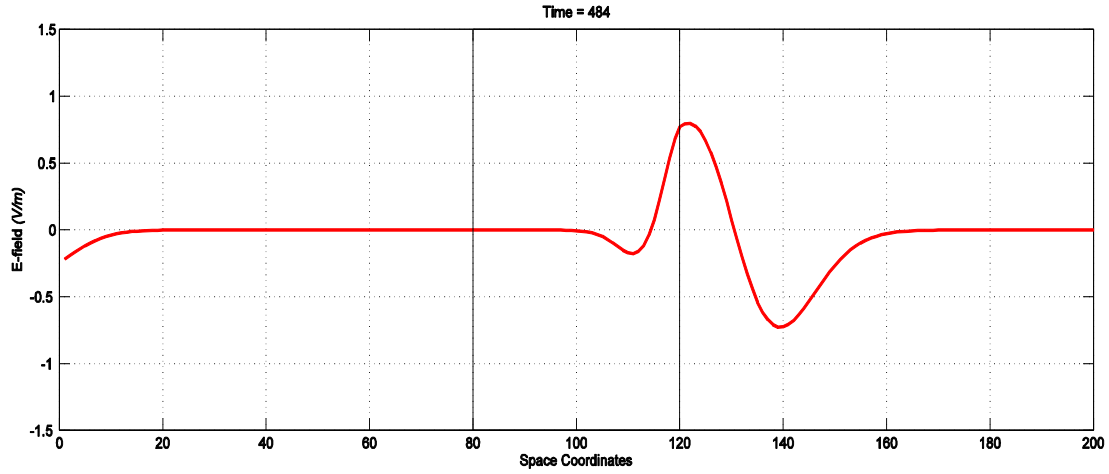

(d) reflection and transmission can be seen at time step=484

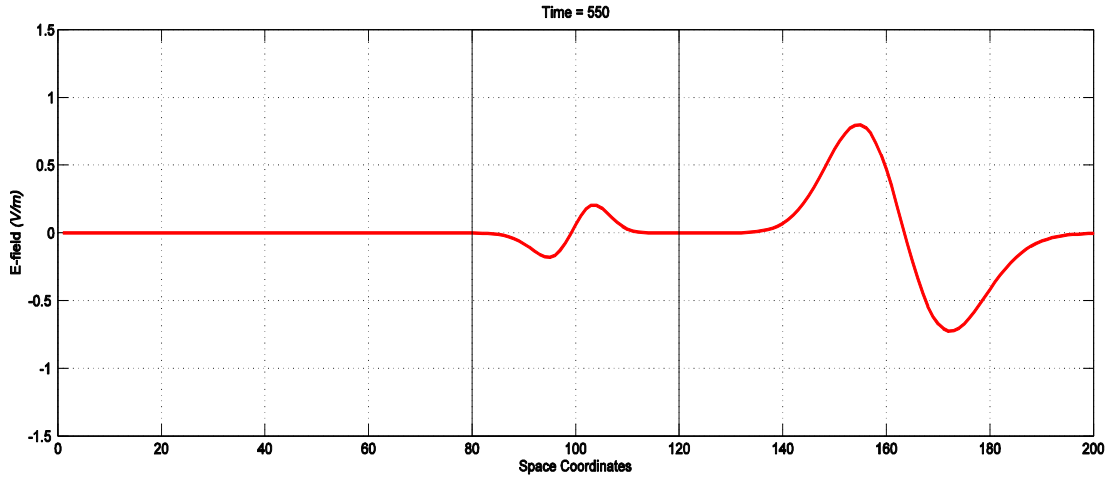

(e) wave increases in amplitude at the end of simulation

Figure 4.2. 1D Simulation of Wave Propagation in Dielectric Slab

Reflections and transmissions of wave propagation in dielectric slab are continuing until it reaches its steady state.

In air-dielectric-air media, relative permittivity and relative permeability of the dielectric slab was defined as 4 and 1, respectively. Therefore, refractive index of the dielectric slab is $n=\sqrt{4}$ which caused reflection and transmitted waves that decreased in amplitude in the slab.

As it is seen, according to discretized forms of Maxwell's equations with different relative permittivity and relative permeability, wave behaviors in different media were observed.

For metamaterial, refractive index of the metamaterial slab is negative. This is causing a backward wave in metamaterial slab due to the negative index of refraction.

4.3 1D Simulation of Metamaterial

The 1D FDTD wave propagation program has been modified for metamaterial simulation. In 1D FDTD air-metamaterial-air wave interaction program, some coefficients such as permittivities, permeabilities, stability criterion, and cell sizes were defined. A metamaterial slab has been defined in the middle of the computational domain and parameters were defined according to the materials.

The discretized forms of Maxwell's equation (eqn's 2.16&2.17) were used as explained in Section 2.1.

In this program, the metamaterial slab has been defined with parameters approaching to ε=-1, μ=-1. The step size is chosen to be Δx=37.7 mm. The time step size is obtained by using the stability criterion as $\Delta t=\Delta x/2c$ as stated in Section 2.4.

For consistency, parameters used in air-dielectric-air media wave propagation simulation were same as air-metamaterial-air media excluding the relative permittivity and permeability in the slab.

The simulation was successful in observing a backward wave at the air-metamaterial interface. As explained before this is a result of negative refractive index.

Simulation results are given at different time steps as shown in Figure 4.3:

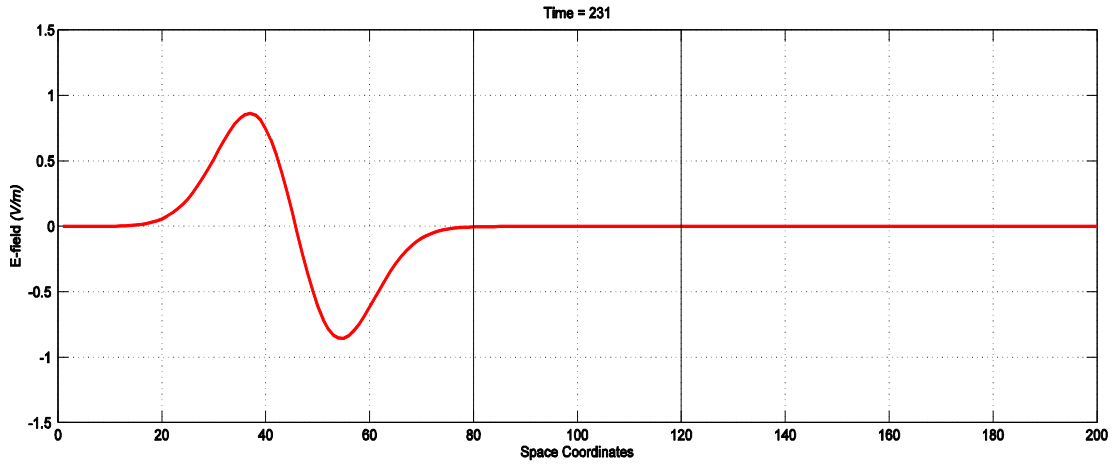

(a) wave starts to propagate in air medium

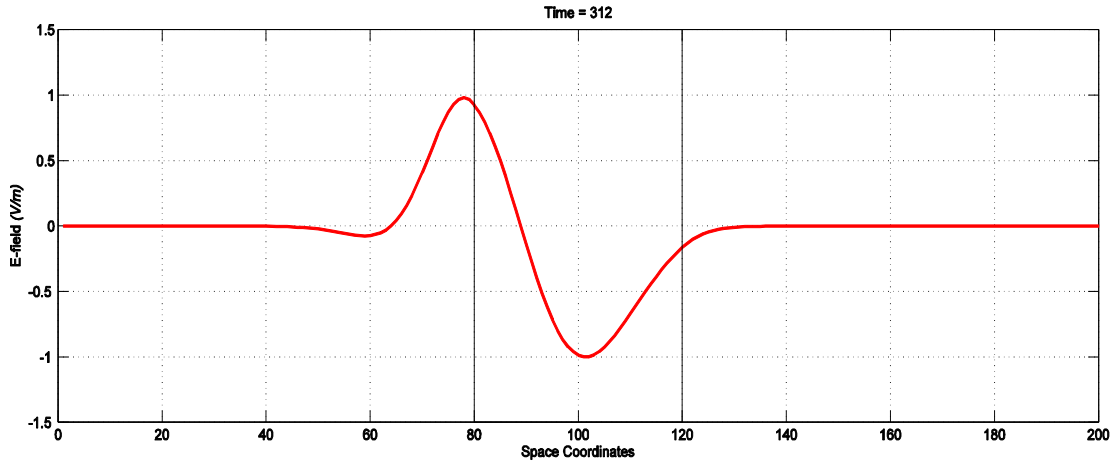

(b) at that time step, wave hits the metamaterial slab

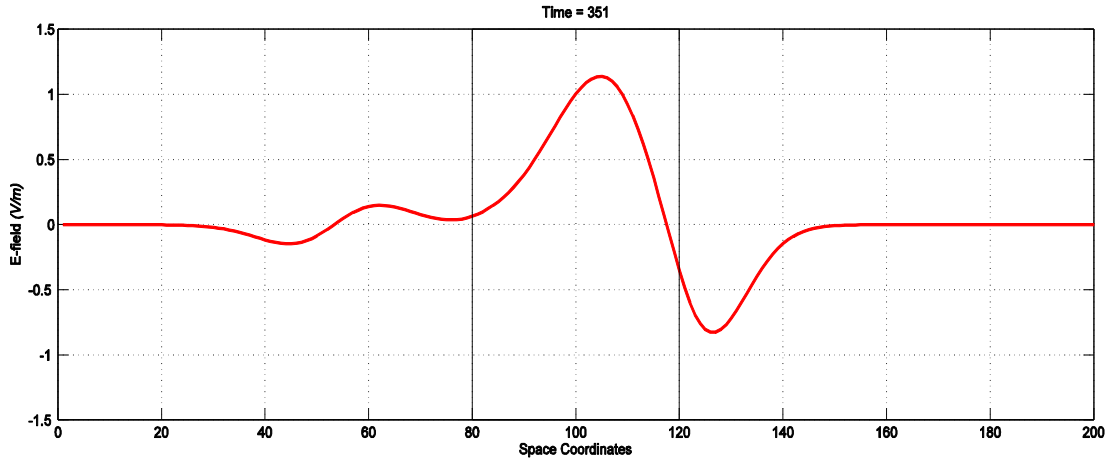

(c) wave is propagating in the metamaterial slab and increases exponentially

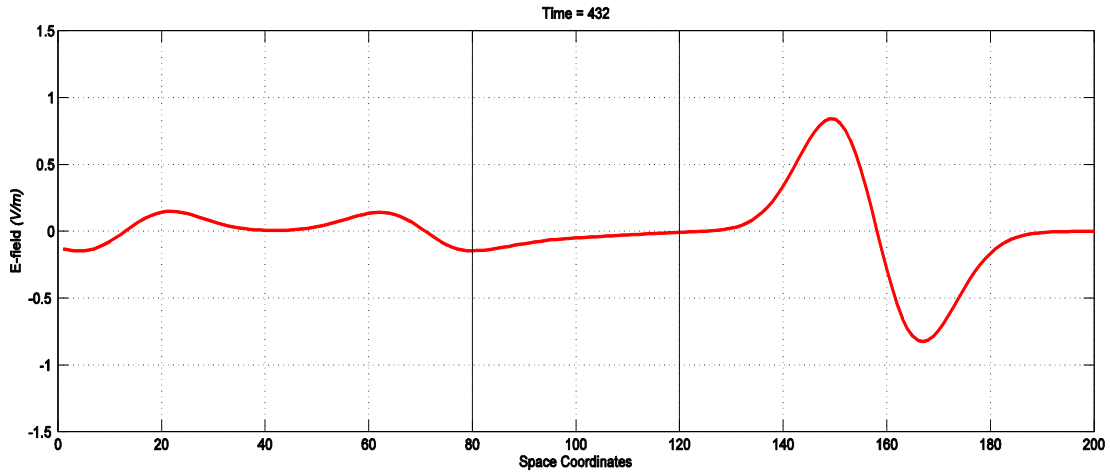

(d) wave nearly returns to its original form and a backward wave occurs

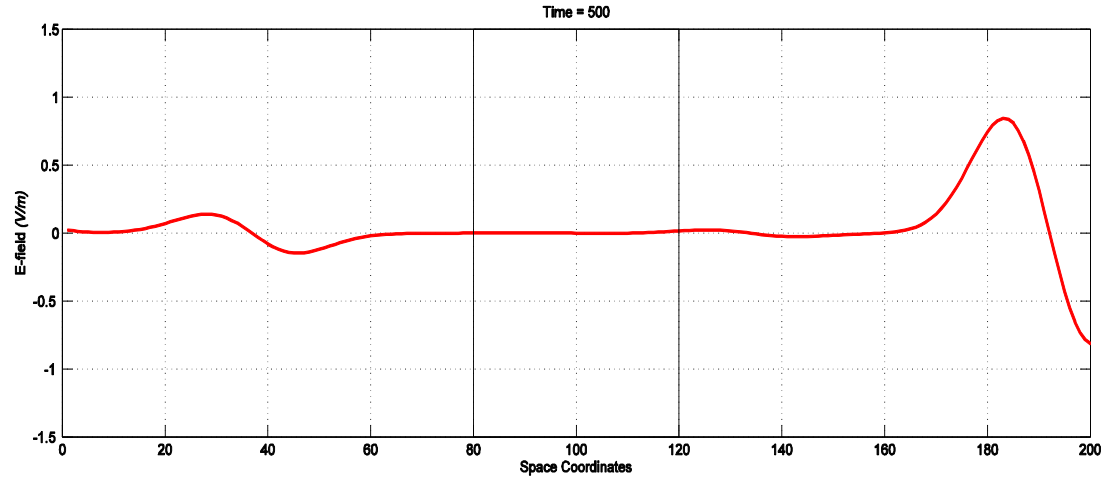

(e) wave returns to its original form as expected

Figure 4.3. 1D Simulation of Wave Propagation in Metamaterial Slab

This simulation means that wave propagation after it passed through metamaterial slab takes its original form as it was at the beginning of the simulation. Wave growth was exponential within the slab and exponential decay was observed outside the slab. The expected backward wave was viewed in the 1D simulation which was found to be consistent with literature [17].

Collin, R.E. [17] explains how reflection and transmission occurs inside the slab by referring to Pendry's study. This study showed that propagating plane wave in the air medium would perfectly matched at the interface and reflection coefficient would be equal to zero and transmission coefficient would be equal to one. This means that fields would go to infinity. In order to solve this, Pendry suggested that taking relative values of permittivity and permeability as both approach to -1 and demonstrated solution as a geometric series which was summation of multiple reflected waves inside the slab. Results showed that full transmission occurred through the slab and wave was exponentially growing inside the slab.

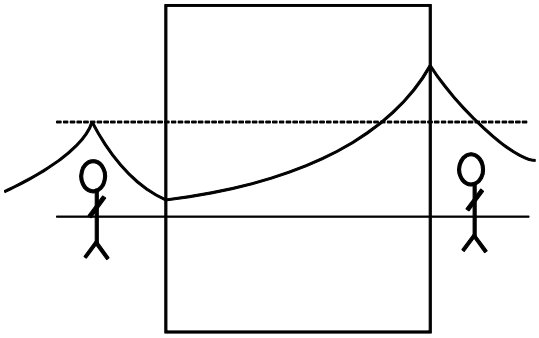

Figure 4.4. Metamaterial Slab [17]

Figure 4.4 shows that the wave is coming through the object and hits the metamaterial slab and then increases exponentially inside the slab and returns its original form after leaving the slab at same distances before and after the slab and image is real.

However, the other LHM effect like perfect lens behavior needs at least a 2D simulation [18].

4.4 2D Simulation of Metamaterials

The 2D FDTD virtual tool has been used to observe the behavior of an electromagnetic wave in an air-metamaterial-air media. The tool selected to be used in this thesis was MTM-FDTD tool which was created by Levent Sevgi [19].

Here scenarios were set to see the difference between the effects of different negative refractive index slabs and also to simulate the perfect focusing of the metamaterials acting as Pendry said a “perfect lens”.

For consistency and accurate comparison, all of the simulations for observing wave behavior include DNG slabs with each of them having negative refractive index, constant slab thickness, same distance from the source and same frequency. The source was defined as Gaussian pulse. Computational domain was defined as 1000x500 cells. The cell sizes are 0.015mm in both directions. The operating frequency was taken as 6 MHz. The selection of computational domain and changing in negative refractive indexes were dependent on the problem of concern. Details are given in Appendix E.

3 scenarios were studied using point source. In scenario 1, the refractive index was chosen to be -6. The slab thickness d and distance from the point source was set as d/2 as seen in Table 4.1. The wave behavior for this case can be seen in Figure 4.5.

The other two scenarios, scenario 2 and scenario 3, were similarly set but with a slab refractive index equal to -2 and -1, respectively. The wave behavior for these cases can be seen in Figures 4.6 and 4.7.

Perfect focusing was observed with a slab that had a refractive index set as -1, less focusing in scenario 2 where the slab refractive index was -2 and minor focusing in scenario 1 where the slab refractive index was -6.

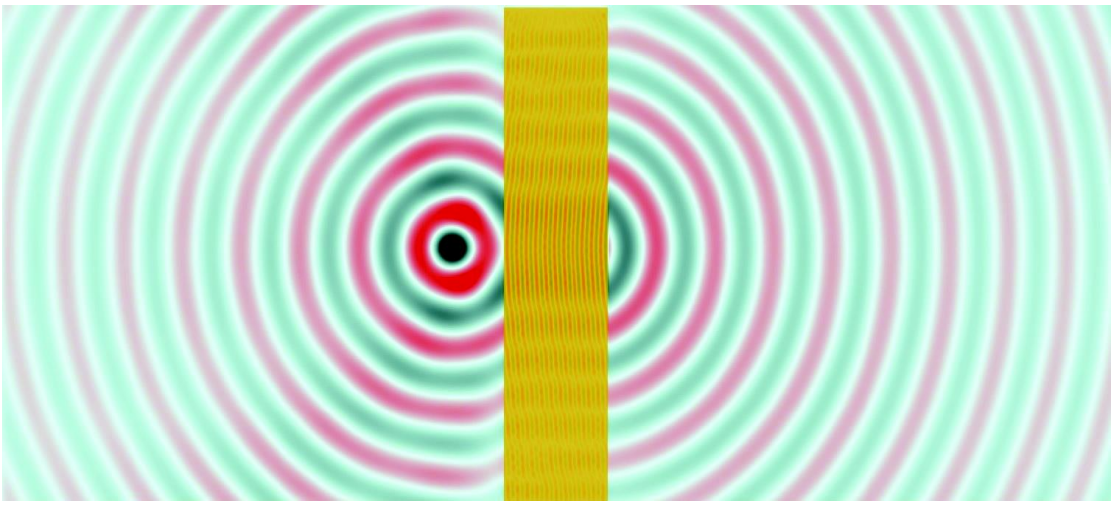

Figure 4.5. Scenario 1: Wave Propagation from a Medium with *n*=-6

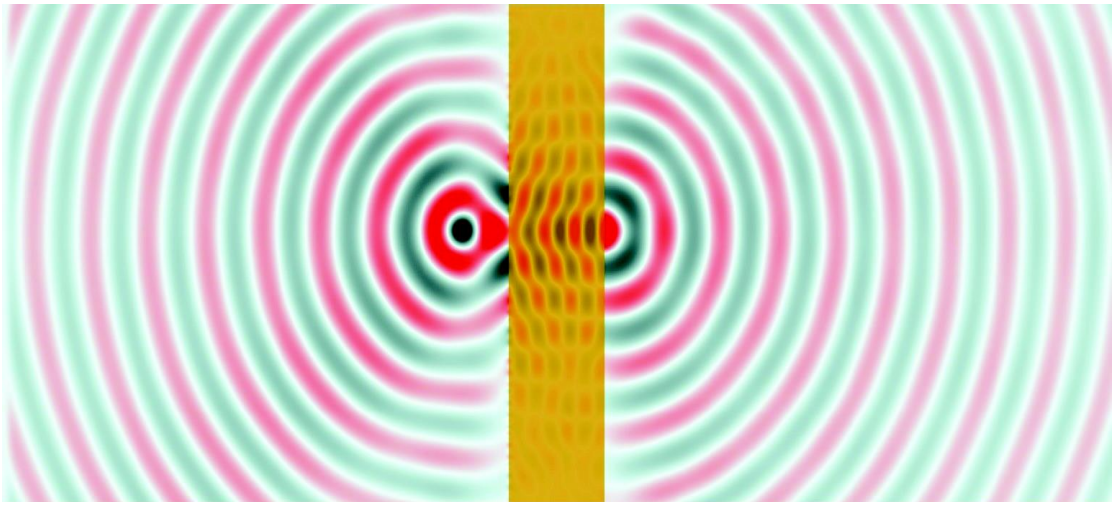

Figure 4.6. Scenario 2: Wave Propagation from a Medium with n=-2

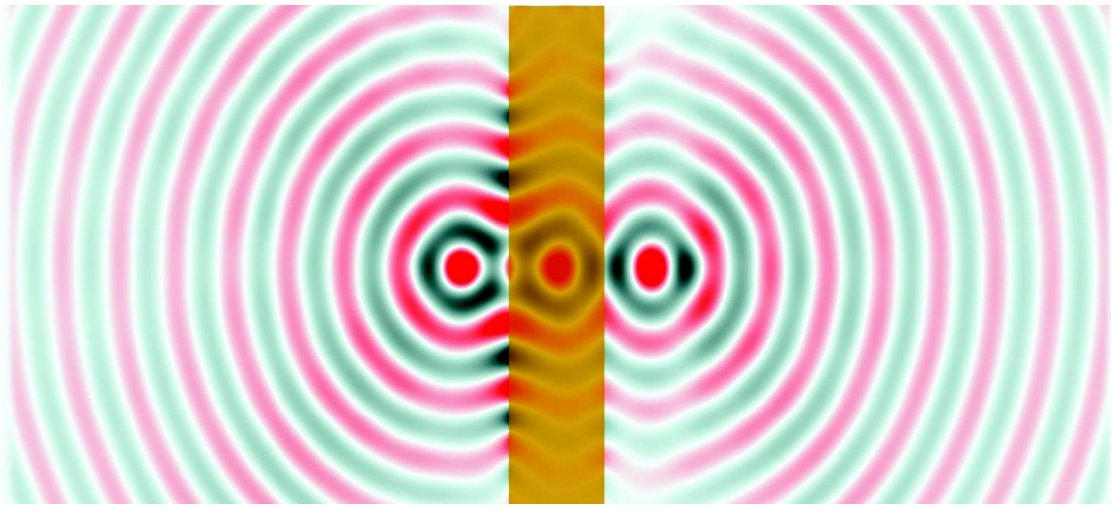

Figure 4.7. Scenario 3: Wave Propagation from a Medium with *n*=-1

Table 4.1. Parameters Used for Simulations with Point Source

Scenarios	**(st)**	**(ssd)**	***N***
Scenario 1	$\lambda/20$	$\lambda/40$	-6
Scenario 2	$\lambda/20$	$\lambda/40$	-2
Scenario 3	$\lambda/20$	$\lambda/40$	-1

st: slab thickness, sd: source-slab distance, *n*: refractive index

The simulation results for the uniform plane source are shown in Figures 4.8, 4.9 and 4.10 and the parameters used in each scenario are given in Table 4.2. Again the slab with refractive index -1 (Figure 4.10 scenario 6) acts as a perfect lens where perfect focusing occurs in the middle of the slab and focusing at a distance d/2 from the slab.

Less focusing was observed in scenario 5 (Figure 4.9), and minor focusing in scenario 4 (Figure 4.8).

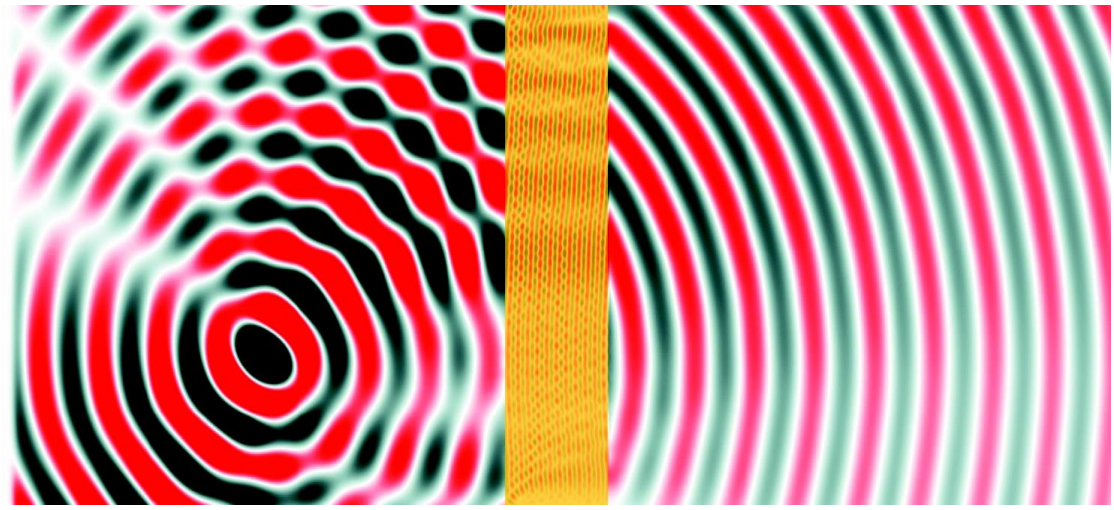

Figure 4.8. Scenario 4: Wave Propagation from a Medium with *n*=-6

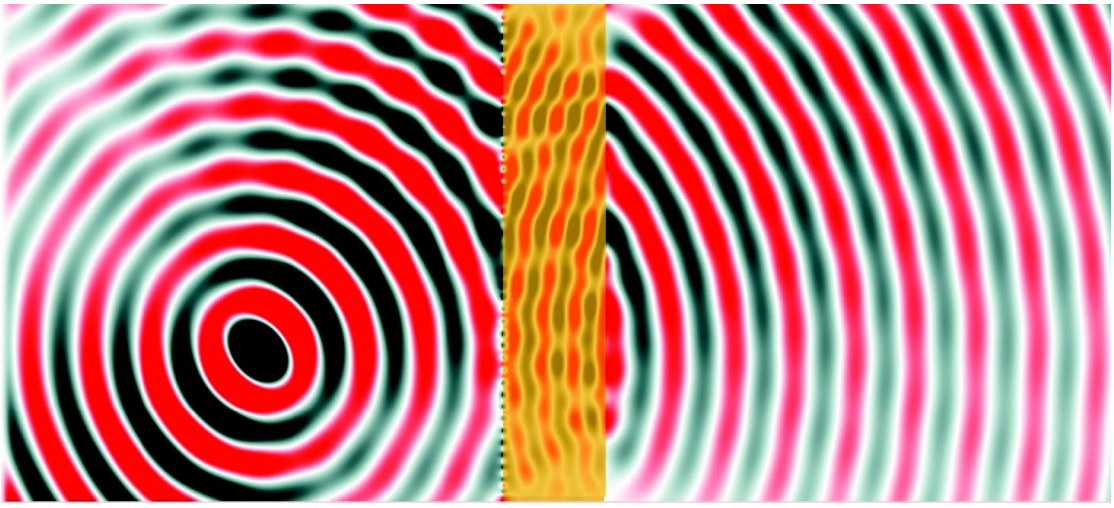

Figure 4.9. Scenario 5: Wave Propagation from a Medium with *n*=-2

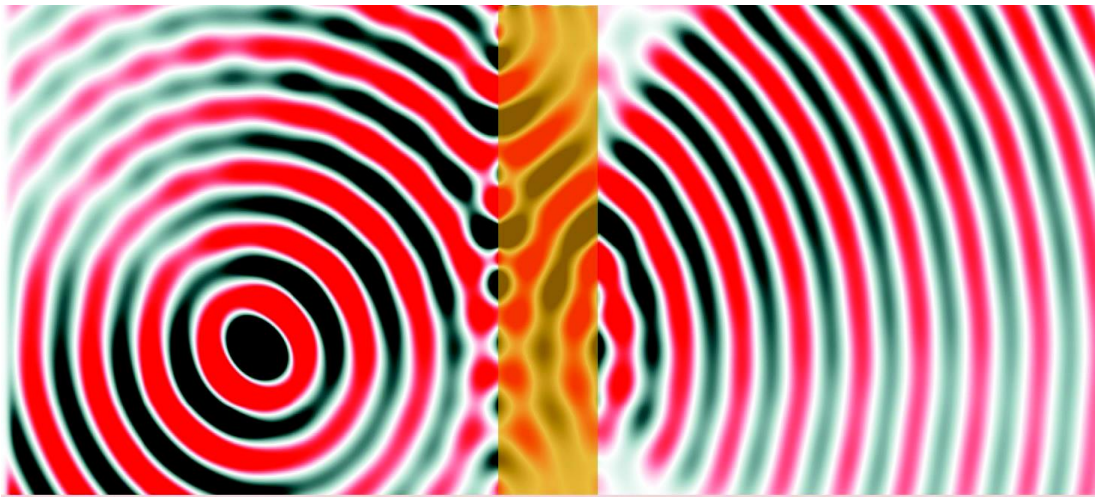

Figure 4.10. Scenario 6: Wave Propagation from a Medium with *n*=-1

Table 4.2. Parameters Used for Simulations with Uniform Plane Wave

Scenarios	**st**	**ssd**	***N***
Scenario 4	$\lambda/20$	$\lambda/40$	-6
Scenario 5	$\lambda/20$	$\lambda/40$	-2
Scenario 6	$\lambda/20$	$\lambda/40$	-1

st: slab thickness, sd: source-slab distance, *n*: refractive index

The last two scenarios (scenario 7 and 8) were studied with double slabs and a point source. The parameters used for these simulations can be seen in Table 4.3. In scenario 7 (Fig. 4.11) two slabs were located at a distance d/2 to the point source, one of them to the left with refractive index -1 and the other to the right of the source with refractive index -2 and with the same slab thickness d.

The difference between the metamaterial slab that acts as a perfect lens and a metamaterial slab with a different negative refractive index can be observed in the same window.

Finally, the 8th scenario was set with two slabs similarly located as in scenario 7 but both with refractive index -1. Both slabs behave as a superlens as seen in Figure 4.12.

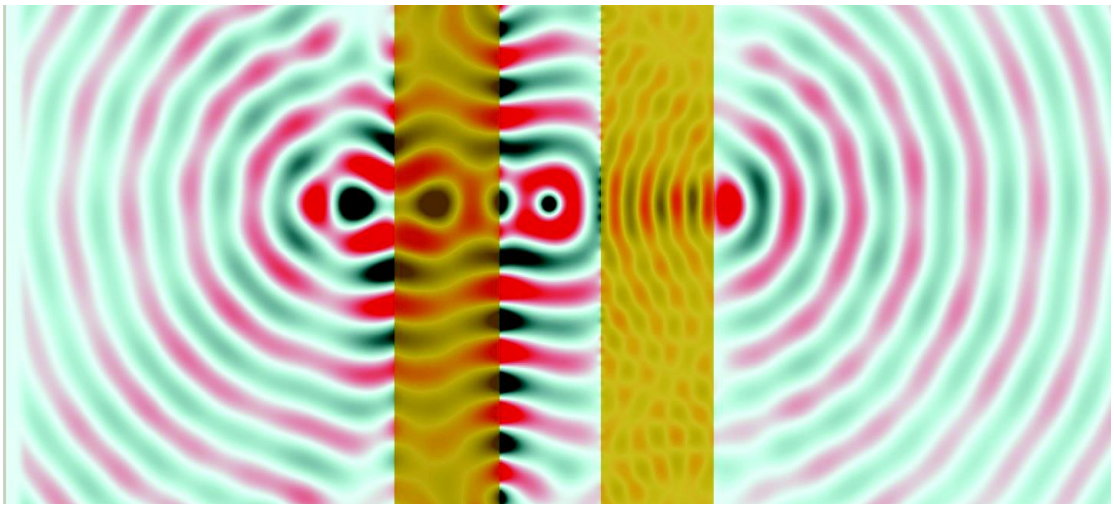

Figure 4.11. Scenario 7: with Slabs *n*=-1 and *n*=-2

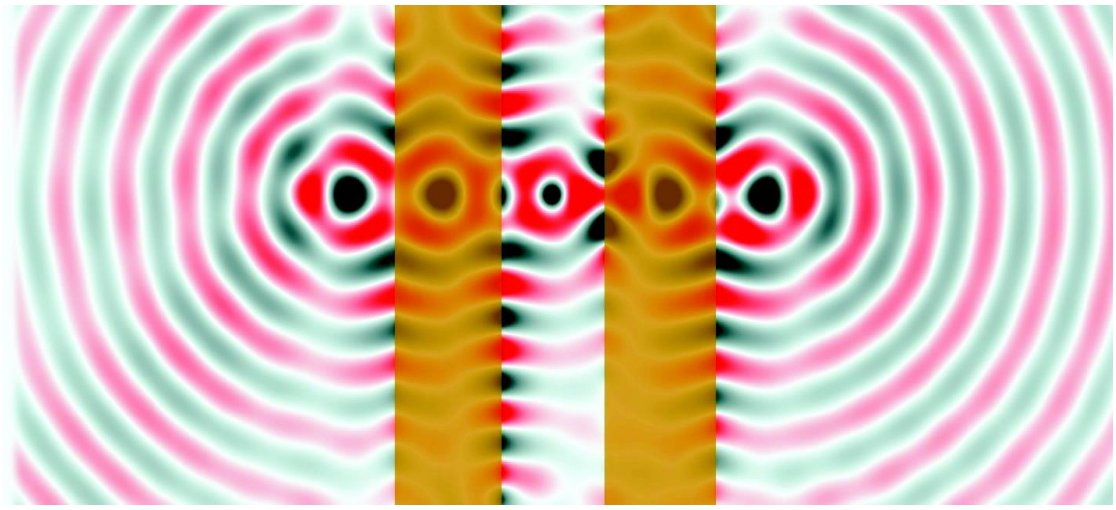

Figure 4.12. Scenario 8: with Slabs *n*=-1 and *n*=-1

Table 4.3. Parameters Used for Simulations with Point Source and Double Slab

Scenarios	Left Slab			Right Slab		
	st	**Ssd**	***n***	**st**	**Ssd**	***n***
Scenario 7	$\lambda/20$	$\lambda/40$	-1	$\lambda/20$	$\lambda/40$	-2
Scenario 8	$\lambda/20$	$\lambda/40$	-1	$\lambda/20$	$\lambda/40$	-1

st: slab thickness, sd: source-slab distance, *n*: refractive index

The study done in this thesis is found to be consistent with that done by Levent Sevgi [19]. Sevgi explained and tried different scenarios in his study by clearly demonstrating the difference between positive and negative refractive indexes. Slab thicknesses were generally taken as 1 cm, source to slab distances was 0.5 cm and frequency was 1 GHz for double-positive media and for metamaterials frequency was 6 MHz Computational domain was defined as 701x351 cells. The cell sizes of 1mm in each direction.

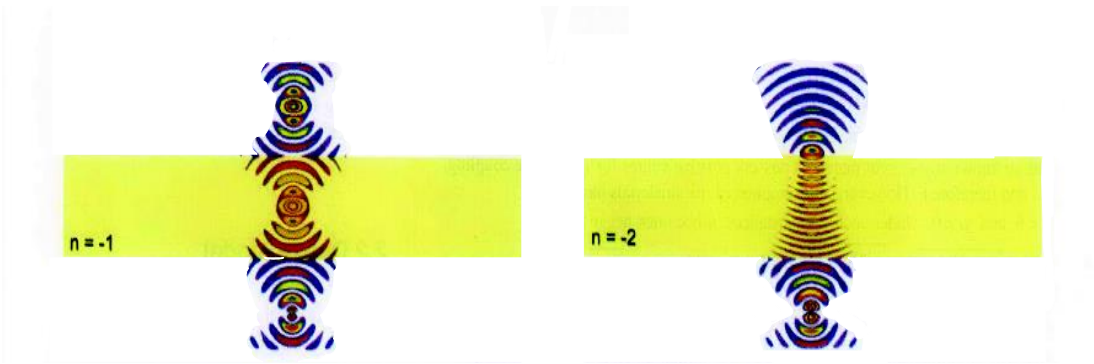

Figure 4.13. Propagation through DNG slabs with *n*=-1 and *n*=-2 [19]

Perfect focusing can be seen in the first figure on the left in Figure 4.13 with refractive index -1 and less focusing is seen in the second figure on the right with refractive index -2.

Richard W. Ziolkowski [20] studied DNG slabs with another FDTD simulator where the computational domain was defined as 600x200 cells, slab thickness 200 cells and the distance between the point source to slab 100 cells with the cell sizes of 1mm. The scenarios studied in this thesis were also found to be consistent with Ziolkowski's work.

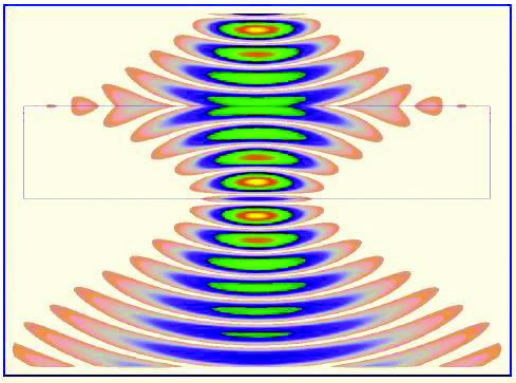

Figure 4.14. DNG Slab with refractive index n=-1 [20]

Figure 4.14 demonstrates that with refractive index -1, backward wave occurred inside the metamaterial slab and perfect focusing was reached.

In this study, source to slab distance was 0.75 cm, slab thickness was 1.5 cm, and computational domain was 1000x500 cells.

All scenarios studied with the point source were found to be consistent with the work done by Levent Sevgi and Richard Ziolkowski and for uniform plane wave, focusing

differences related with source and negative refractive index observed inside the metamaterials slab.

Chapter 5

CONCLUSIONS

In this thesis, the simulation of wave behavior in metamaterials has been investigated. 1D and 2D simulations of metamaterials have been carried out by using the FDTD method. 1D simulation of wave propagation in dielectric and metamaterial slabs has been coded in Matlab. For 2D simulations, FDTD tools in literature were investigated and FDTD based virtual tool compatible with metamaterials were selected to observe the 2D wave behavior within negative refractive index materials.

The 1D FDTD wave propagation through air-dielectric-air media were studied for comparison with the wave behavior in air-metamaterial-air media. The relative permittivity and relative permeability of the dielectric slab was defined as 4 and 1, respectively; therefore, refractive index of the dielectric slab is positive. This caused reflection and transmitted waves that decreased in amplitude in the slab. In 1D simulation of metamaterial, the refractive index of the metamaterial slab is negative (-1), the relative permittivity and relative permeability are chosen as approaches to -1 each. The negative refractive index caused a backward wave in the metamaterial slab. The observation of a backward wave in the simulation was successful. Also as expected there was no reflection. Wave growth was exponential within the slab and exponential decay was observed outside the slab. The expected backward wave was viewed in the 1D simulation which was found to be consistent with the literature but

since other LHM effects like perfect lens behavior needs at least a 2D simulation, for this purpose 2D simulations were studied.

Different scenarios were studied to observe the wave behavior in various negative refractive index materials. The slab thicknesses and source-slab distances were selected as suggested by Pendry with the aim of obtaining a perfect focus inside the slab and a wave same as that sent by the source d/2 away, after the slab. A perfect focus was observed only in scenario 3, scenario 6 and scenario 8, where metamaterial slabs were used with refractive index -1. In scenario 7, one of the slabs has refractive index -1 and the other -2. This gives the opportunity to compare the change of the wave behavior in metamaterials as refractive index decreases in the same computational domain.

The study done in this thesis is found to be consistent with that done by Levent Sevgi. Sevgi explained and tried different scenarios in his study by clearly demonstrating the difference between positive and negative refractive indexes. Slab thicknesses were generally taken as 1 cm, source to slab distances was 0.5 cm and frequency was 1 GHz for double-positive media and for metamaterials frequency was 6 MHz Computational domain was defined as 701x351 cells.

In the present thesis, parameters are defined as slab to source distance was 0.75 cm, slab thickness was 1.5 cm, and computational domain was 1000x500 cells with 0.015 mm cell size.

All scenarios studied with the point source were found to be consistent with the work done by Levent Sevgi and for uniform plane wave, focusing differences related with

source and negative refractive index were observed inside the metamaterial slab. This study can be extended to include the design and experiments of each scenario.

Richard W. Ziolkowski studied DNG slabs with another FDTD simulator where the computational domain was defined as 600x200 cells, slab thickness 200 cells and the distance between the point source to slab 100 cells with the cell sizes of 1mm. The scenarios studied in this thesis were also found to be consistent with Ziolowski's work.

According to these results, one can say that metamaterials can be used as a perfect lens. The results obtained can be used for further research and can form a background for realizing 3D simulations. Research on understanding metamaterials and their potential use will continue to be a hot topic for a long time.

REFERENCES

[1] J. B. Pendry, A. Holden and W. Stewart, "Extremely Low Frequency Plasmons in Metallic Mesostructures," *Phys. Rev. Lett.*, vol. 76, no. 25, pp. 4773-4776, 1996.

[2] J. B. Pendry, A. Holden, D. Robins and W. Stewart, "Magnetism from Conductors and Enhanced Nonlinear Phenomena," *IEEE Trans. Microw. Theory Tech.*, vol. 47, p. 2075, 1999.

[3] V. G. Veselago, "The Electrodynamics of Substances with Simultaneously Negative Values of ε an μ," *Sov. Phys. Usp.*, vol. 10, pp. 509-514, 1968.

[4] R. A. Shelby, D. R. Smith and S. Shultz, "Experimental Verification of a Negative Index of Refraction," *Science*, vol. 292, p. 77, 2001.

[5] K. Yee, "Numerical Solution of Initial Boundary Value Problems Involving Maxwell's Equations in Isotropic Media," Antennas and Propagation, IEEE Transactions, vol. 14, no. 3, pp. 302-307, 1966.

[6] M. N. O. Sadiku, Elements of Electromagnetics, New York: Oxford University Press, 2001.

[7] A. Taflove and S. Hagness, Computational Electrodynamics: The Finite-Difference Time-Domain Method, Artech House, Incorporated, 2005.

[8] G. Mur, "Absorbing Boundary Conditions for the Finite-Difference Approximation of the Time-Domain Electromagnetic-Field Equations," *IEEE Transactions on Electromagnetic Compatibility Society*, vol. EMC, no. 23, pp. 377-382, 1981.

[9] J. B. Pendry and D. R. Smith, "The Quest for the Superlens," *Scientific American*, pp. 60-67, 2006.

[10] "Metamorphose VI AISBL," 9 February 2013. [Online]. Available: http://metamorphose-vi.org/index.php?option=com_content&view=category&id=43&Itemid=137.

[11] A. Sihvola, "Metamaterials in Electromagnetics," *Science Direct*, pp. 2-11, 2007.

[12] N. Engheta and R. W. Ziolkowski, Metamaterials Physics and Engineering Explorations, USA: IEEE Press, 2006.

[13] R. Uyguroğlu, "Reflection and Refraction," in *Electromagnetics II Lecture Notes*, Eastern Mediterrenean University Famagusta, 2013.

[14] D. K. Cheng, Fundamentals of Engineering Electromagnetics, Addison Wesley Publishing Company Incorporated, 1992.

[15] F. E. Resource. [Online]. Available: http://www.citycollegiate.com/image_formation_convex.htm. [Accessed 3 November 2013].

[16] J. B. Pendry, "Negative Refraction Makes a Perfect Lens," *Physical Review Letter,* vol. 85, p. 3966, 2000.

[17] R. E. Collin, "Frequency Dispersion Limits Resolution in Veselago Lens," *Progress in Electromagnetics Reseach B,* vol. 19, pp. 233-261, 2010.

[18] R. Marques, J. Martel, F. Mesa and M. F, "A New 2D Isotropic Left-Handed Metamaterial Design: Theory and Experiment," *Microwave and Optical Technology Letter,* vol. 35, no. 5, pp. 405-408, 2002.

[19] M. Çakır, G. Çakır and L. Sevgi, "A Two-Dimensional FDTD-Based Virtual Visualization Tool for Metamaterial-Wave Interaction," *IEEE Antennas and Propagation Magazine,* vol. 50, no. 3, pp. 166-175, 2008.

[20] R. W. Ziolkowski, "Pulsed and CW Gaussian Beam Interactions with Double Negative Metamaterial Slabs," *Optics Express,* vol. 11, no. 7, pp. 663-681, 2003.

APPENDICIES

Appendix A: Historical Development of Metamaterials

The origins of the latest metamaterial research go back to 1904 when Schuster showed that a wave incident in media that allows a backward wave will go “the wrong way”. The medium mentioned here is a medium that supports waves that have phase and group velocities opposed to each other. Most articles, including review articles on metamaterials miss to mention studies before Veselago therefore it is worth giving a chronology of the important work that lead to metamaterials. (That is the foundation of metamaterials).

Chronology of developments that lead to metamaterials:

- 1904 Schuster: As explained above, Schuster stated that when a wave is propagating in a media that allows backward waves will go the wrong way.
- 1905 Pocklington: In a medium that allows backward waves, when a source is activated, a wave is generated with phase velocity directed toward the source and with group velocity directed in the opposite direction.
- 1914 Lindman: Known to be the first to show the effect of chiral medium on electromagnetic waves. The developments including different methods and approaches later were directly transferred to metamaterial research.
- 1945 Mandelshtam: Stated that negative refraction occurs in a medium that supports backward waves.
- 1951 Malyuzhinets: About 45 years later rediscovered Pocklington’s result.
- 1957 Sivukhin: Discussed in media with negative refractive index, there will be some general properties related with wave propagation.

- 1967 Veselago: Studied the properties of metamaterials by emphasizing that there is no natural material with simultaneously negative permittivity and permeability and by focusing on answering the question "what kind of properties would such a medium have?" (medium with both ε and μ negative) Veselago called the medium having simultaneously negative permittivity and permeability, left-handedness and negative refractive index materials.
- 1996 Pendry: Showed that a metallic rod or rodded structures have negative permittivity ($\varepsilon<0$) and plasma like behavior.
- 1999 Pendry: Showed that split ring resonators (SRR) can be used for negative permeability ($\mu<0$).
- 2000 Smith: About 35 years later after Veselago's findings they fabricated metamaterials. Materials with negative refractive index. They used split ring resonator, thin straight wires previously studied and introduced by Pendry to make a material with negative permittivity and negative permeability.
- 2000 Pendry: Showed that Veselago's plane-parallel lens is capable of subwavelength imagining and introduced the term "perfect lens" since metamaterials have negative refractive index and have the ability of perfect focusing.
- 2001 Shelby: Proved that the material fabricated by Smith el al had a negative refraction. This study was the first experimental verification of materials with negative refractive index.

Appendix B: Applications of Metamaterials

Pendry's perfect lens is known to be the first application of metamaterials. After metamaterials fabrication by research groups turned their focus to metamaterials. In the past decade, enormous research took place in this field and promising studies are going on related with its applications. Work on inventing usable technology is continuing in some fields as antennas, microwave absorbers, medical devices, radar systems, imaging systems and even cloaking devices, MSA-T (metamaterials surface antenna technology) is a recently invented product that is planned to be commercialized in 2015.

Appendix C: Matlab Code for Dielectric Slab

```
max_time = 600;
Ex=zeros(1,200);
Hy=zeros(1,200);
IE=zeros(1,max_time);
mu0=4*pi*10^-7;
dx=0.0377;
dt=dx/(6e8);
f=2*10^9;
w=2*pi*f;
e0=8.854e-12;
er=4;
mr=1;
alpha1=dt/(e0*er*dx);
alpha2=dt/(mu0*mr*dx);
%ABC
E_low_m2=0;
E_low_m1=0;
E_high_m2=0;
E_high_m1=0;
spread=25;
t0=150;
T=0;
for n=1:max_time
    T=T+1;
```

```
    for k=2:200
       if(k<80)
          er=1;
       Ex(k)=Ex(k)+(dt/(e0*er*dx))*(Hy(k-1)-Hy(k));
       elseif(k>=80&&k<=120)
        er=4;
      Ex(k)=Ex(k)+(dt/(e0*er*dx))*(Hy(k-1)-Hy(k));
       else
          er=1;
         Ex(k)=Ex(k)+(dt/(e0*er*dx))*(Hy(k-1)-Hy(k));
       end
    end
    pulse=-2.0*((t0-T)./spread).*exp(-1.*((t0-T)./spread)^2);
       Ex(5)=Ex(5)+pulse;
     if(k >=50 && k <=90)
        er=4;
        Ex(k)=Ex(k)+alpha1*(Hy(k-1)-Hy(k));
     else
        er=1;
        Ex(k)=Ex(k)+alpha1*(Hy(k-1)-Hy(k));
     end
  end
% Boundary Condition
    Ex(1) =E_low_m2;
    E_low_m2=E_low_m1;
```

```
    E_low_m1=Ex(2);
    Ex(200)=E_high_m2;
    E_high_m2 = E_high_m1;
    E_high_m1 = Ex(200 - 1);
for j=1:200-1
    Hy(j)=Hy(j)+alpha2*(Ex(j)-Ex(j+1));
end
     for j=1:200-1
     if(j >=50 && j <=90)
         mr=1;
         else
             Hy(j)=Hy(j);
         end
    end
     figure(1)
    plot(Ex,'r','LineWidth',2);
    rectangle('Position',[80,-1.5,40,3],'LineWidth',2,'LineStyle','--')
    grid on
    xlabel('Space Coordinates');
    ylabel('E-field\it{(V/m)}');
    axis([0 200 -1.5 1.5])
    title(['Time = ',num2str(n)]);
    pause(0.05)
end
```

Appendix D: Matlab Code for Metamaterial Slab

```
max_time = 500;

E=zeros(1,200);

D=zeros(1,200);

B=zeros(1,200);

H=zeros(1,200);

S=zeros(1,200);

S1=zeros(1,200);

S2=zeros(1,200);

I=zeros(1,200);

I1=zeros(1,200);

I2=zeros(1,200);

IE=zeros(1,max_time);

RE=zeros(1,max_time);

TE=zeros(1,max_time);

Eif=zeros(1,max_time);

Erf=zeros(1,max_time);

Etf=zeros(1,max_time);

RC=zeros(1,max_time);

TC=zeros(1,max_time);

S11=zeros(1,max_time);

S21=zeros(1,max_time);

mue=4*pi*10^-7;

dx=0.0377;

dt=dx/(6e8);
```

```
foe=0.15915e9;

fom=0.15915e9;   % f= frequency

fpe=1.1027e9;

fpm=1.1027e9;  % f= frequency

wp=2*pi*fpe;

f=0.7957e9;

w=2*pi*f;

e0=8.854e-12;

taue=0.0;

taum=0.0;

e2=-0.0099;

e1=-0.0099;

omegae=2*pi*foe;

omegam=2*pi*fom;

dele=taue/(2*omegae);

alpha=omegae*dele;

gama=square(2*pi*fpe)/((2*pi*foe).*sqrt(1-dele));

beta=(2*pi*foe)/(sqrt(1-dele));

delm=taum/(2*omegam);

alpha1=omegam*delm;

gama1=square(2*pi*fpm)/((2*pi*fom).*sqrt(1-delm));

beta1=(2*pi*fom)/(sqrt(1-delm));

%ABC

E_low_m2=0;

E_low_m1=0;
```

```
E_high_m2=0;
E_high_m1=0;
spread=25;
t0=150;
T=0;
for n=1:max_time
   T=T+1;
   for k=2:200
      D(k)=D(k)+0.5*(H(k-1)-H(k));
   end
  pulse=-2.0*((t0-T)./spread).*exp(-1.*((t0-T)./spread)^2);
   D(5)=D(5)+pulse;
  for k=2:200
   if(k >=80 & k <=120) %#ok<AND2>
      E(k)=(D(k)-S(k))/e2;
      S(k)=((2*exp(-alpha*dt)).*cos(beta*dt).*S1(k))-(exp(-
2*alpha*dt).*S2(k))+((gama).*exp(-alpha*dt).*sin(beta*dt).*e1.*dt.*E(k-1));
      S2(k)=S1(k);
      S1(k)=S(k);
   else
      E(k)=D(k);
   end
end
   % Boundary Condition
   E(1) =E_low_m2;
```

```
    E_low_m2=E_low_m1;
    E_low_m1=E(2);
    E(200)=E_high_m2;
    E_high_m2 = E_high_m1;
    E_high_m1 = E(200 - 1);
     T=0;
for n=1:max_time
     T=T+1;
for j=1:200-1
    B(j)=B(j)+(0.5)*(E(j)-E(j+1));
end
    for j=1:200-1
    if(j >=80 && j <=120) %#ok<ALIGN>
        H(j)=(B(j)-I(j));
        I(j)=((2*exp(-alpha1*dt)).*cos(beta1*dt).*I1(k))-(exp(-
2*alpha1*dt).*I2(k))+((gama1).*exp(-alpha1*dt).*sin(beta1*dt).*e0.*dt.*H(k-1));
        I1(j)=I(j);
        I2(j)=I1(j);
        else
            H(j)=B(j);
        end
    end
    IE(T)=E(20);
    RE(T)=E(59);
    TE(T)=E(90);
```

```
    figure(1)
    plot(E,'r','LineWidth',2);
    rectangle('Position',[80,-1.5,40,3],'LineWidth',2,'LineStyle','--')
    grid on
    xlabel('Space Coordinates');
    ylabel('E-field\it{(V/m)}');
    axis([0 200 -1.5 1.5])
    title(['Time = ',num2str(n)]);
    pause(0.05)
    Eif(T)=fft(IE(T));
    Erf(T)=fft(RE(T));
    Etf(T)=fft(TE(T));
    RC(T)=abs(Erf(T)/Eif(T));
    TC(T)=abs(Etf(T)/Eif(T));
    S11(T)=20*log10(RC(T));
    S21(T)=20*log10(TC(T));
end
```

Appendix E: MTM-FDTD Program

Material type which will be used for simulation is specified first.

Lorentz formulation is used to obtain negative permittivity and negative permeability that can be changed by using “advanced material parameters” window.

Source has to be defined by using the window named “advanced source injection”. Some values such as “num elements, array angle, spacing, amplitude, frequency” are defined inside that window to reach Gaussian pulse in the computational domain.

In addition to this, DNG slab was chosen from the “parameters” window, then it has to be located in the computational domain.

Slabs can be defined as rectangular, ellipse and triangular.

Range and height are already defined in the program. While change the height, range is automatically changing by the half of the height. When height is changed, program is changing the refractive indexes, instantly.

Ex, Ey and Hz components are defined and all of them can be seen in the computational domain by changing it from the “view” window.

Appendix F: MTM-FDTD Iterative Equations

$$F_z\Big|_{i+\frac{1}{2},j+\frac{1}{2}}^{n+\frac{1}{2}} = \frac{2\varepsilon_0 K_z - \sigma_z \Delta t}{2\varepsilon_0 K_z + \sigma_z \Delta t} F_z\Big|_{i+\frac{1}{2},j+\frac{1}{2}}^{n-\frac{1}{2}} + \frac{2\varepsilon_0 \Delta t}{2\varepsilon_0 K_z + \sigma_z \Delta t}\left(\frac{E_x\Big|_{i+\frac{1}{2},j+1}^{n} - E_x\Big|_{i+\frac{1}{2},j}^{n}}{\Delta y} - \frac{E_y\Big|_{i+1,j+\frac{1}{2}}^{n} - E_y\Big|_{i,j+\frac{1}{2}}^{n}}{\Delta x}\right)$$

$$B_z\Big|_{i+\frac{1}{2},j+\frac{1}{2}}^{n+\frac{1}{2}} = B_z\Big|_{i+\frac{1}{2},j+\frac{1}{2}}^{n-\frac{1}{2}} - \frac{2\varepsilon_0 K_z + \sigma_z \Delta t}{2\varepsilon_0} F_z\Big|_{i+\frac{1}{2},j+\frac{1}{2}}^{n+\frac{1}{2}} - \frac{2\varepsilon_0 K_z + \sigma_z \Delta t}{2\varepsilon_0} F_z\Big|_{i+\frac{1}{2},j+\frac{1}{2}}^{n-\frac{1}{2}}$$

$$H_z\Big|_{i+\frac{1}{2},j+\frac{1}{2}}^{n+\frac{1}{2}} = \frac{1}{\mu_0 \mu_\infty}\left(B_z\Big|_{i+\frac{1}{2},j+\frac{1}{2}}^{n+\frac{1}{2}} - \mu_0 \sum_{k=1}^{N} S_{zk}\Big|_{i+\frac{1}{2},j+\frac{1}{2}}^{n+\frac{1}{2}}\right)$$

$$S_{zk}\Big|_{i+\frac{1}{2},j+\frac{1}{2}}^{n+2} = 2\frac{2 - w_{ok}^2 \Delta t^2}{2 + \delta_k w_{ok} \Delta t} S_{zk}\Big|_{i+\frac{1}{2},j+\frac{1}{2}}^{n+1} + \frac{-2 + \delta_k w_{ok} \Delta t}{2 + \delta_k w_{ok} \Delta t} S_{zk}\Big|_{i+\frac{1}{2},j+\frac{1}{2}}^{n} + 2\frac{\alpha_k w_{ok}^2 \Delta t^2}{2 + \delta_k w_{ok} \Delta t} H_z\Big|_{i+\frac{1}{2},j+\frac{1}{2}}^{n+1}$$

$$G_x\Big|_{i+\frac{1}{2},j}^{n+1} = \frac{2\varepsilon_0 K_y - \sigma_y \Delta t}{2\varepsilon_0 K_y + \sigma_y \Delta t} G_x\Big|_{i+\frac{1}{2},j}^{n} + \frac{2\varepsilon_0 \Delta t}{(2\varepsilon_0 K_y + \sigma_y \Delta t)\Delta y}\left(H_z\Big|_{i+\frac{1}{2},j+\frac{1}{2}}^{n+\frac{1}{2}} - H_z\Big|_{i+\frac{1}{2},j-\frac{1}{2}}^{n+\frac{1}{2}}\right)$$

$$D_x\Big|_{i+\frac{1}{2},j}^{n+1} = D_x\Big|_{i+\frac{1}{2},j}^{n} + \frac{2\varepsilon_0 K_x + \sigma_x \Delta t}{2\varepsilon_0} G_x\Big|_{i+\frac{1}{2},j}^{n+1} - \frac{2\varepsilon_0 K_x + \sigma_x \Delta t}{2\varepsilon_0} G_x\Big|_{i+\frac{1}{2},j}^{n}$$

$$E_x\Big|_{i+\frac{1}{2},j}^{n+1} = \frac{1}{\varepsilon_0 \varepsilon_\infty}\left(D_x\Big|_{i+\frac{1}{2},j}^{n+1} - \varepsilon_0 \sum_{k=1}^{N} S_{xk}\Big|_{i+\frac{1}{2},j}^{n+1}\right)$$

$$S_{xk}\Big|_{i+\frac{1}{2},j}^{n+2} = 2\frac{2 - w_{ok}^2 \Delta t^2}{2 + \delta_k w_{ok} \Delta t} S_{xk}\Big|_{i+\frac{1}{2},j}^{n+1} + \frac{-2 + \delta_k w_{ok} \Delta t}{2 + \delta_k w_{ok} \Delta t} S_{xk}\Big|_{i+\frac{1}{2},j}^{n} + 2\frac{\alpha_k w_{ok}^2 \Delta t^2}{2 + \delta_k w_{ok} \Delta t} E_x\Big|_{i+\frac{1}{2},j}^{n+1}$$

$$G_y\Big|_{i,j+\frac{1}{2}}^{n+1} = \frac{2\varepsilon_0 K_x - \sigma_x \Delta t}{2\varepsilon_0 K_x + \sigma_x \Delta t} G_y\Big|_{i,j+\frac{1}{2}}^{n} - \frac{2\varepsilon_0 \Delta t}{(2\varepsilon_0 K_x + \sigma_x \Delta t)\Delta x}\left(H_z\Big|_{i+\frac{1}{2},j+\frac{1}{2}}^{n+\frac{1}{2}} - H_z\Big|_{i-\frac{1}{2},j+\frac{1}{2}}^{n+\frac{1}{2}}\right)$$

$$D_y\Big|_{i,j+\frac{1}{2}}^{n+1} = D_x\Big|_{i,j+\frac{1}{2}}^{n} + \frac{2\varepsilon_0 K_y + \sigma_y \Delta t}{2\varepsilon_0} G_y\Big|_{i,j+\frac{1}{2}}^{n+1} - \frac{2\varepsilon_0 K_y - \sigma_y \Delta t}{2\varepsilon_0} G_y\Big|_{i,j+\frac{1}{2}}^{n}$$

$$E_y\Big|_{i,j+\frac{1}{2}}^{n+1} = \frac{1}{\varepsilon_0 \varepsilon_\infty}\left(D_y\Big|_{i,j+\frac{1}{2}}^{n+1} - \varepsilon_0 \sum_{k=1}^{N} S_{yk}\Big|_{i,j+\frac{1}{2}}^{n+1}\right)$$

$$S_{yk}\Big|_{i,j+\frac{1}{2}}^{n+2} = 2\frac{2 - w_{ok}^2 \Delta t^2}{2 + \delta_k w_{ok} \Delta t} S_{yk}\Big|_{i,j+\frac{1}{2}}^{n+1} + \frac{-2 + \delta_k w_{ok} \Delta t}{2 + \delta_k w_{ok} \Delta t} S_{yk}\Big|_{i,j+\frac{1}{2}}^{n} + 2\frac{\alpha_k w_{ok}^2 \Delta t^2}{2 + \delta_k w_{ok} \Delta t} E_y\Big|_{i,j+\frac{1}{2}}^{n+1}$$